



*Facultad
de
Ciencias*

**EARTH-STOPPING OF MILLICHARGED
DARK MATTER**
(Efecto de frenado terrestre sobre Materia
Oscura ‘Milicargada’)

Trabajo de Fin de Grado
para acceder al

GRADO EN FÍSICA

Autor: Joaquín Merino Areitio

Director: Bradley James Kavanagh

Septiembre - 2021

Agradecimientos

Aquí se acaban 4 años (+ un verano extra) de carrera. Es muy cliché lo que voy a decir pero sí, se han pasado volando. Y sin embargo, en esta etapa tan aparentemente fugaz he conocido a grandes personas, a las que me gustaría incluir en estos agradecimientos.

Antes que nada, por supuesto, agradeceré a mis padres. Desde que entré a la carrera, dos personas que han sido siempre los máximos exponentes de las letras en casa, han comenzado a interesarse por la actualidad en física o incluso se han enganchado a ver vídeos divulgativos. Y las conversaciones que surgen de ahí, y en general de cualquier lado, son siempre interesantes, y dejan un buen sabor de boca. Gracias por apoyarme todos estos años desde la distancia, aunque yo muchas veces no me haya dejado. Gracias también a Lucía, que aunque también lejos, sé que siempre estará ahí, tanto para hablar de banalidades como también de cosas más serias.

En segundo lugar, gracias a los de la Meseta. Vine a Santander con miedo de no encontrar a un grupo de gente con la que llevarme bien y, en cambio, encontré a personas que, pese a ser bien distintas entre sí, siempre consiguieron que encontrara un hueco en el que estar a gusto.

Gracias en especial a la ISS: Gracias a Senior y a sus inolvidables duchas por la mañana con la música a tope. Gracias a Unai por saber un poco de todo, pero de todo! Y, por supuesto, a Pablo, por las tan necesarias dosis de humor irreverente y... ejem.

Quería agradeceré en especial a tí, Elena. Si hay un motivo por el cual yo he podido seguir adelante todos estos años sin tirarme demasiado de los pelos, ha sido por que has estado siempre a mi lado, apoyándome hasta en el momento más duro. Muchas gracias.

And last but not least, I would like to thank Bradley for his tutoring. He has been very supportive from the beginning of the project, and has always helped me whenever I needed to with any question I had, while at the same giving me the freedom required to produce this kind of projects. Thanks a lot for your patience!

Abstract. One of the most prominent open problems in modern cosmology is the identification of the nature of Dark Matter (DM), a kind of matter which is apparently invisible and only manifests itself strongly through gravitational effects which have had the scientific community intrigued throughout the past few decades. Up to now, no Standard Model particle has been able to fully describe the properties of DM so, at the moment, there are plenty of beyond Standard Model particles proposed as candidates to be constituents of DM. In particular this project is focused on one of them: *millicharge* DM particles, which have a very small electric charge, much smaller than that of an electron.

The existence of these particles within the DM Halo surrounding our Galaxy would mean that there exists a certain flux of *millicharged* DM (mcDM) which is going through the Earth, and right into our detectors. In its path, the DM particles may interact with the different nuclei species on Earth, which makes them slow down, or even stop. This 'Earth-stopping' effect may give rise to an interesting new time-varying signals once the particles reach the detector so, in this project, the 'Earth-stopping' effect is thoroughly studied in the framework of direct detection, by initially analyzing the situation for the conventional, electrically neutral DM, and then analyzing it for the *millicharge* case. Then, the time varying signals corresponding to both DM scenarios are calculated for detectors located at different places on Earth, and buried at different depths. The signals are compared, and it is discussed whether this is a valid comparison method.

Key words: dark matter, direct detection, millicharged dark matter, earth-stopping effect, annual modulation.

Resumen. Una de las cuestiones abiertas más relevantes en la cosmología moderna es la identificación de la naturaleza de la Materia Oscura, un tipo de materia que es aparentemente invisible y que tan solo se manifiesta fuertemente mediante efectos gravitatorios, que han tenido a la comunidad científica intrigada durante décadas. Hasta ahora, no ha habido ninguna propuesta válida de partícula desde el Modelo Estándar, con lo que existen numerosas propuestas fuera de este modelo y, particularmente, este proyecto se centra en una de dichas propuestas: la materia oscura *milicargada*, una partícula con una carga eléctrica mucho más pequeña que la de un electrón.

La existencia de estas partículas en el Halo de materia oscura que nos rodea significaría que existiría un cierto flujo de estas partículas atravesando la tierra, y llegando a nuestros detectores. En su camino, la partícula de materia oscura podría interactuar con los núcleos terrestres, de tal manera que pudiera ser frenada o incluso parada totalmente. Este 'efecto de frenado terrestre' podría dar lugar a nuevas señales dependientes del tiempo una vez que las partículas frenadas llegaran a los detectores. En este proyecto este efecto de frenado se estudia concienzudamente en el marco de la detección directa de materia oscura, analizando primero la situación para materia oscura convencional, para luego pasar a la materia oscura *milicargada*. Luego, las señales temporales asociadas a cada uno de los dos escenarios se calculan para detectores en distintas localizaciones y profundidades. Las señales correspondientes se comparan, y se discute si esta manera es una forma válida de compararlas.

Palabras clave: materia oscura, detección directa, materia oscura milicargada, efecto de frenado terrestre, modulación anual.

Contents

1	Introduction	1
1.1	The dark matter hypothesis: First evidences	2
1.2	Current DM status	4
1.2.1	Detection of DM	5
1.2.2	Alternatives to DM: Modified gravity	6
1.3	Dark matter candidates	7
1.3.1	General properties	7
1.3.2	Proposed particles	8
1.4	Objectives and structure of this project	9
2	Direct detection of Dark matter	11
2.1	Direct detection formalism	11
2.1.1	Derivation of the differential recoil rate, $\frac{dR}{dE_R}$	12
2.1.2	Derivation of the recoil energy	13
2.1.3	Spin-independent DM-nucleus differential cross section	14
2.1.4	Form factor correction	15
2.2	Understanding the DM Halo	17
2.2.1	Local DM density, ρ_0	17
2.2.2	Velocity distribution: Standard Halo Model (SHM)	17
2.2.3	SI recoil spectra for the Maxwellian distribution	18
2.2.4	Earth's motion and time dependence of the signal	20
2.3	Nuclear stopping of DM on Earth	22
2.3.1	Coordinate system	25
2.3.2	Velocity transfer	25
2.3.3	Speed distribution at the detector	27
2.4	Standard DM velocity distributions	28
3	Direct detection of <i>Millicharged</i> Dark Matter	30
3.1	An overview on the candidate	30
3.1.1	<i>Millicharged</i> DM-nucleus differential cross section	30
3.2	<i>Millicharged</i> recoil spectra for the Maxwellian distribution	32
3.3	Nuclear stopping of <i>millicharged</i> DM on Earth	33
3.3.1	Velocity transfer	34
3.4	<i>Millicharged</i> DM velocity distributions	35
4	Signal analysis. Constraints and proposed detectors	37
4.1	Time-dependence of the differential recoil rate	37
4.2	Time-varying SI and <i>millicharge</i> signals	38
4.2.1	Signals for various detectors and analysis	39
4.3	Constraints	41

5 Discussion and conclusions

43

Bibliography

44

Chapter 1

Introduction

Understanding the Universe and the way in which it evolves is definitively one of the major open problems in modern physics. Within this gigantic problem it is of course particularly interesting to study the constituents that build up the Universe that we live in. Currently we can only identify approximately the 20% of its total matter content, with the remaining 80% [1] being an unknown substance whose origin is uncertain, which makes its existence apparent only via gravitational effects, but that apparently does not interact with conventional matter via the electromagnetic force, hence being invisible at any wavelength.

To investigate the nature of this so-called Dark Matter (DM) has thus become one of the main priorities in the quest of characterizing the Universe, and it comes as no surprise that, given that no Standard Model (SM) particle could be found to describe a substance such as DM, many beyond SM particles have been proposed as DM candidates that would correlate with this rather strange, but yet abundant, matter. This work revolves around one particular proposal: ***Millicharged Dark Matter (mcDM)*** - particles of DM which have a very small electric charge, much smaller than the charge of an electron. Current constraints indicate that, if this proposal is in fact a reasonable candidate, it would only contribute a small fraction to the DM population (what is usually referred to as a sub-dominant contribution), though it is not yet discarded. It is thus necessary for new experiments to try and detect this kind of particles or at least probe in some way the currently available parameter space in which mcDM is still a valid candidate.

It has to be remarked that no experiment today has been able to directly or indirectly detect a certain DM candidate; rather, they put limits in the possible values of different properties of the different candidates, such as their mass. As is to be expected, the list of proposed ways and ongoing experiments that try to detect DM candidates is not exactly short. In this project, **direct detection** techniques are explored to try and find a differentiating signature that would indicate towards the detection of one of these *millicharged* particles over any other type of DM candidate, in view of proposing new detectors that may exploit this signature.

Particularly, one would expect these particles to be populating the galactic DM halo and - given the motion of the Earth relative to the galactic rest frame - to find them travelling through our home planet, leaving a possible signal at a sufficiently sensitive detector. However, we must take into account that these DM particles may interact with electrons and nuclei in the Earth in their path to the detector. These interactions can slow and even stop the incoming DM particles, modifying the signal in the process. This effect, which we will refer to as **Earth-stopping** is sensible to differentiate a mcDM signal from an 'ordinary DM' signal, due to the fact that the interaction cross section of each of the two types of DM has a different dependence

on the recoil energy imparted to the stopping nuclei. Naturally, this effect is time dependent, due to the aforementioned relative motion of the Earth, and this fact may open a window to explore differentiating properties of the DM signal left by a *millicharged* particle, as opposed to a conventional, electrically neutral, DM particle.

In this context, the project explores the Earth-stopping effect for both ordinary and *millicharged* DM, in order to extract the form of the corresponding **time-varying signals**, and then compare them, in the hope of finding this characteristic signature that would differentiate them both. This study is going to be made in the low DM mass regime (sub-GeV to a few GeV range). The reasoning behind that decision is that, usually, the limits on the parameter space of heavy Dark Matter are already strong (their possible properties are already quite constrained), so there is not really much available interesting space for us to explore the Earth-scattering effect in.

Once the signal analysis has been carried out, the goal would be to explore the existing literature to determine which constraints exist for mcDM and whether there exist regions of the currently available parameter space which can in fact be probed in future proposed detectors.

The remaining pages of the introduction aim to contextualize Dark Matter historically and observationally, giving some early and also some more up-to-date evidences of its existence, as well as to talk about methods of detection, and about particles and other objects which have been presented as candidates to be constituents of Dark Matter.

1.1 The dark matter hypothesis: First evidences

In 1933, Swiss astronomer Fritz Zwicky published a paper on the redshift of extragalactic nebulae [2] in which he particularly commented on the Coma cluster's velocity dispersion. By making the assumption that the nebulae cluster had already reached a mechanically stationary state (following a process commonly referred to as virialization) he came to the conclusion that, for Coma to be stable, its average density would have to be ~ 400 times greater than that derived from the observations based on luminous matter. The author then attributed this issue to the presence of a yet unseen, dark, matter (*'dunkle Materie'*), which greatly exceeded the luminous matter content of the galaxy cluster.

He then proceeded to examine three other possibilities:

1. The cluster may have not been in a virialized state yet. This scenario still needed a great deal of dark matter to be consistent.
2. Analyze the high velocity dispersion measured for the cluster by assuming that its average density was only due to the observed luminous matter (and not due to a dark matter component). If that were the case, and the speeds were in fact real, the nebulae would be flying apart from the cluster at speeds on the order of $\mathcal{O}(10^3)$ km/s. One would thus expect that, at the evolutionary state of the Universe at that time, more individual nebulae would have been observed with such large speeds, but this was not at all the case, the typical speeds of these objects having been measured to be somewhere around 200 km/s.
3. Analyze the high velocity dispersion by assuming that measured speeds were not real, but rather a consequence of Einstein's redshift. However, this required even more DM presence to be consistent.

It was clear that the inconsistency found by Zwicky posed a staggering problem in physics: What was this *dark matter*? Why was it so apparently abundant, and yet no other signal or observation had led to a similar hypothesis? Despite the interesting nature of Zwicky's proposal, serious scientific debate regarding the discrepancies found in an increasing number of galaxy clusters did not occur until the late 1950s [3]. These debates extended up until the early 1970s, and the possible explanations for the aforementioned discrepancies were numerous and varied in character; from a large presence of gravitational radiation to a need to change the law of gravity, never discarding the possibility of observational errors.

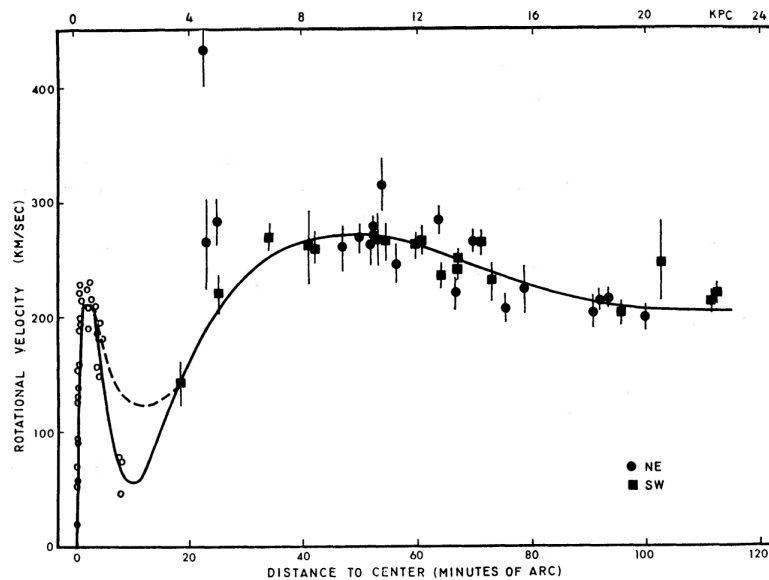


Figure 1.1. *Optically studied rotation curve of ionized hydrogen in the Andromeda galaxy (M31), Rubin and Ford [4].*

In 1970, Vera Rubin famously published, together with Kent Ford, an study on the rotation curves that could explain the measured rotational velocities of the spiral galaxy M31 [4].

Spiral galaxies are basically rotating flat disks of matter. If this disk has a uniform distribution of matter, and we were to measure the velocity from the centre of the disk as a function of the radial distance, we would find that the velocity increases with the radius: the points furthest away from the centre and the ones next to it do a full rotation in the same time, so the former set of points must travel at higher orbital speeds. This can be understood in terms of the mass enclosed inside the radius of each orbit: more mass inside the orbit means more orbital speed. However, if we take a look at a spiral galaxy, we would see that the centre of the astronomical object is way more luminous than its exterior regions, so we would assume that most of the mass of the galaxy is concentrated at its centre region. If that is true, then there will be a radial distance beyond which, the mass enclosed by increasing orbital radius would remain almost constant, which means that the orbital velocity of external material necessarily decreases with distance.

So, based on the distribution of luminous matter, a declining behaviour of the rotational velocities was expected for sufficiently large radial distances. However, they found that, in fact, the curve flattened as the radius increased (see figure 1.1), which meant that more gravity was present in the galaxy than that corresponding to the observed luminous matter. From that point on, other studies [3] which acknowledged this flattening issue appeared, and it was beyond doubt that it posed an open problem in the field.

A change in the general research interests of astronomers and physicists directed the focus of the scientific community to extragalactic phenomena, Einstein's general relativity and cosmology, which in turn made the correct determination of the mass of galaxies and galaxy clusters a very important issue [3]. This ultimately led to both of the aforementioned observations - anomalously high velocity dispersions and flat rotation curves at high radial distances in spiral galaxies - becoming the first independent evidences for the existence of DM.

1.2 Current DM status

The rather slippery properties of DM have made it quite difficult to characterize. Numerous probes and constraints, which are later to be mentioned, have built up the general consensus that DM must be a non-baryonic kind of matter, with nearly neutral electromagnetic behaviour (otherwise, it would be able to somehow interact with light and this, in principle, should have been already detected) and which has negligible velocities (cold dark matter or CDM). Concerning the latter, it has long been excluded for all DM to have a large velocity dispersion [5], as this would entirely contradict the knowledge that we have on structure formation; objects such as the galaxies we observe, and live in, would have not been able to gravitationally collapse, and, thus, form, had the DM velocity dispersion been large enough. It is to be acknowledged that some degree of freedom is left to accept astrophysical / cosmological models which include modest velocity dispersions for DM but here we will focus on the benchmark assumption that the DM is, indeed, cold.

The previous assumptions are encompassed within the Λ CDM cosmological model, which describes the universe as a perturbed Friedmann-Lemaître-Robertson-Walker (FLRW) flat space-time with dynamics satisfying Einstein's equations [5]. It is the most accepted cosmological model given the goodness of its fit to the measured data. This kind of models present a certain set of 'density' parameters, with each representing a particular property of the universe, such as:

- Its matter content: baryonic matter (Ω_b) and Dark Matter Ω_c .
- Its radiation density (Ω_γ).
- Its dark energy density (Ω_Λ) (responsible for the accelerated expansion).

Λ CDM is just the cosmological model which uses the least number of cosmological parameters, without compromising the goodness of its description regarding the observational data.

According to the high precision measurements of the cosmic microwave background (CMB) anisotropies (see figure 1.2) made by the *Planck* collaboration [1], DM accounts for approximately the 25% of the critical density of the universe, which in turn means that it accounts for more than 80% of the total matter density.

This large component of the total matter density of the universe is observed to be present in gravitationally collapsed structures, ranging in size from small galaxies to galaxies as big as the Milky Way, and also on bigger structures such as clusters. Backing up the previously mentioned early evidences for the existence of DM, a great deal of modern independent observations have made its presence in these collapsed structures even more apparent.

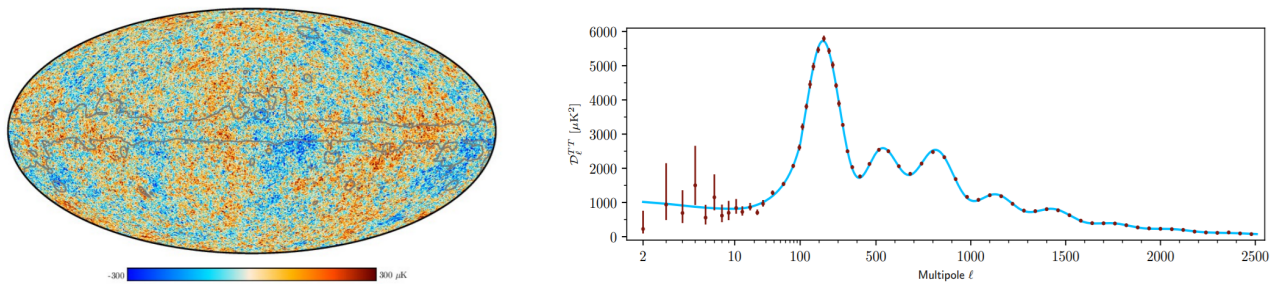


Figure 1.2. (left) CMB temperature map (2018 SMICA). (right) Planck CMB power spectrum for temperature.

Within these structures, DM is inferred by comparing measurements of the corresponding total baryonic, non DM, mass (stellar number counts and measures of gas densities through X-Ray emission) and measurements of the total mass enclosed inside a given radius, which can be achieved with the already mentioned mass tracers: rotation curves in structures similar to spiral galaxies, stellar velocity dispersions, virialized systems, etc. [5] On top of this, there are other techniques, such as gravitational lensing. This is the effect by which light apparently bends around massive astronomical objects, such as the clusters of DM, due to their large gravitational pull, able to heavily curve space-time. The latter is considered one of the best probes that the scientific community has regarding the dark sector, and it has vitally contributed to the establishment of various properties now taken for granted for DM, such as the fraction that it represents over the total mass content of the universe, its nearly electrically neutral behaviour and also its distribution throughout the universe, which is not in the form of planet-sized dense structures, but rather in the form of big haloes [6].

Also, and as has been briefly mentioned before, the current model for structure formation heavily supports the DM hypothesis, the dark matter being the scaffolding in the whole process of gravitationally collapsing the big scale structures that are visible nowadays [5].

1.2.1 Detection of DM

In the present work, **direct detection techniques** are going to be explored and used in order to study DM. These kinds of experiments aim to detect DM candidates through the signal that they leave as recoil energy in the detector's nuclei after scattering off them. The formalism needed to study these signals and the corresponding analysis is gone through in subsequent chapters, so no more discussion regarding direct detection will be given here in the introduction.

It is interesting though to acknowledge other forms of detection of DM, and their relevance in the DM paradigm. In the same line as the previously mentioned observations and arguments, lies the astrophysical detection of DM, a manifestation of the discipline of **indirect detection**. The latter is focused on studying the debris left behind of an **annihilation** or **decay** process from a pair of DM particles or, respectively, a single DM particle. Here we will only briefly mention a few ways in which these processes can be tracked down.

- **Gamma rays:** In the event of an annihilation occurring, gamma rays are emitted in almost every scenario, with independence of the final state of the whole process [5] and, thus, these gamma rays are usually studied in the search of a bright DM signal. These searches are usually carried out around specific targets that ensure one of two things. The first one is that a low

background (better SNR) is expected for that specific target in the energy ranges in which gamma rays are relevant. An example of this are dwarf spheroidal galaxies - [7] combines the gamma ray data gathered for 15 dSphs in a 6-year observation span using the Large Area Telescope, providing very strong constraints in the annihilation cross section of DM. The other thing is that the DM density is large enough, like the inner region of our own galaxy. However, this is in general rather problematic, as the galactic centre is very bright in almost every wavelength, giving large backgrounds. On the other hand, decay processes involving gamma rays may be better studied in nearby clusters of galaxies with high enough astrophysical emission.

- **Neutrinos:** DM particles may get captured inside celestial bodies such as the Sun, if the precise requirements on scattering cross section and magnitude of flux of incident DM are met. If enough DM is captured to the point that the density of DM particles inside the celestial body is greater than the mean DM density in the galactic halo, self annihilation of those particles inside the astronomical object may become relevant enough to leave a Standard Model particle track behind which can be followed [8]. In particular, highly energetic neutrinos are produced in this kind of situation, and they are able to escape the sun, thus being liable to be detected here on Earth. The fact that those neutrinos are more energetic than solar neutrinos, makes this a nearly background-free channel for DM search.

- **Anti-matter cosmic rays:** DM particles can decay directly (or indirectly, first decaying to an intermediate state) to a range of charged particles. In order to improve SNR, experiments are usually conducted for rare species of particles such as positrons or antiprotons. These experiments usually focus on analyzing an excess of this kind of particles in numerous astrophysical scenarios [5]. Some of these searches have been successful in finding the aforementioned excesses (for example [9]). However, contradicting evidence, constraints from other experiments, other non-DM related explanations and the presence of numerous systematic errors have made the assertion of ascribing these measurements to Dark Matter somewhat controversial.

Other way in which DM may be detected is through the study of DM signals in particle **colliders / accelerators**. The corresponding analysis is usually carried out under the assumption that the DM particles interact very weakly with the material of the detector, escaping the detector and leaving behind missing amounts of energy and momentum, similar to the results obtained when amongst the final state particles there are neutrinos [5]. This is only one way in which particle colliders are able to probe the dark sector; however, no DM signal has been detected to date in colliders / accelerators and, thus (for the moment), these experiments only provide limits on couplings, cross sections and masses related to the vast zoo of DM candidate particles included in a long list of numerous beyond-SM models. These limits, naturally, do not provide definite conclusions on whether the probed candidates are in fact a good enough description of DM, and they need to be cross-checked with direct detection experiments in order to extract meaningful information [10].

1.2.2 Alternatives to DM: Modified gravity

It is worth acknowledging that alternative models to DM have been proposed, most prominently the ones which make use of a modified law of gravity to explain the gravitational effects that are otherwise attributed to this new, yet uncategorized, beyond Standard Model, substance. Even though these proposals may cover the same effects as those attributed to the presence of DM, they do it in a very limited range of scales, failing to do so in greater ones, and encountering problems when predicting some observations such as the anisotropies in the power spectrum of

the CMB [5].

One of the most prominent measurements which is favourable to the DM hypothesis and at the same time completely inconsistent with the modified gravity models, is the bullet cluster (see 1.3).

As can be readily seen from figure 1.3, there is a significant offset between the centroid of the mass distributions calculated through gravitational lensing and the gas bullet, prominently emitting in X-rays. This is contrary to what one would expect from modified gravity models, which would place the lensing mass peak at the gas distribution, as it is the dominant visible (baryonic) mass component [11].

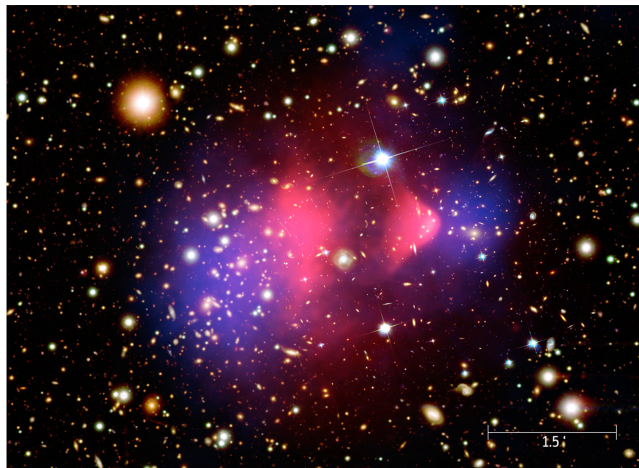


Figure 1.3. Composite image showing 1E 0657-56, the bullet cluster. X-ray image (pink, recorded by Chandra Telescope) superimposed over a visible light image (galaxies), with matter distribution calculated from gravitational lensing (blue).

Thus, the DM proposal still stands out for being the one that solves the most problems, even though a great deal of work has yet to be done in further constraining its properties, in order for its nature to be better understood.

1.3 Dark matter candidates

Although we have already mentioned some properties that the DM is accepted to present, it is useful to gather all of this information in one place so both these properties and also the proposed DM candidates are well understood.

1.3.1 General properties

We can say that, for a particle to pose as a candidate for DM, it has to comply with the following requirements.

They have to **match** their corresponding **relic density** (that is, the number density of the particle at the time of freeze-out in the early universe), they have to be **stable**: the lifetime of the candidate must be long when compared to cosmological timescales [12], and be **cold** - as required from structure formation, as previously mentioned.

Also, the candidate must be compatible with constraints on **self-interaction** cross sections coming from observations of merging clusters or ellipticity measurements of certain galaxies through the study of X-Ray emission [5]. Of course, it also has to be compatible with other kind of experiment and / or phenomena, such as **direct detection** experiments or **stellar evolution**.

Regarding its mass, lower and upper limits can be given through observation of various astrophysical events.

For **fermionic** candidates, the **lower mass bound** can be found from observations of the velocity dispersion and physical density of dwarf galaxies [5], giving a fermionic mass above **70eV**. On the other hand, the **lower mass bound on bosonic** candidates has been worked out through observations of CMB and large-scale structure, Lyman- α observations and measurements of high-redshift galaxy luminosity functions [5], giving a bosonic mass above **10^{-22} eV**.

In the case of **upper bounds on the mass**, we have that, assuming a point-like DM candidate which constitutes the totality of DM, the mass of this constituent would be at most **$5M_{\odot}$** [13].

Finally, and regarding the DM **neutrality**, even though it is common to state that DM does not interact electromagnetically with matter, thus its invisibility in every wavelength, really there is room for the DM to be slightly charged, much less than a unit of electron charge. These would be the *millicharged* DM particles. It has been found [14] that the most rigorous constraints come from the requirement that the DM was completely decoupled from the baryon-photon plasma at recombination. We will talk about constraints in the *millicharge* in subsequent chapters.

1.3.2 Proposed particles

In this field it is common to put forward candidates that either are embedded in a theoretical framework that solves an open issue in particle physics, or that come from ad-hoc models, built specifically to try to explain some experimental / observational result [5]. Amongst the long list of proposed DM particles, we are going to highlight the following:

- **WIMP**: Weakly Interacting Massive Particles, they usually are the preferred model, because it arises from models which address the hierarchy problem (related to the great discrepancy between the Electro-Weak force and gravity), and also readily explain the observed relic abundance [5].
- **Axions**: They were introduced to solve the CP violation problem in particle physics, and have later become relevant as a possible DM candidate. Several experiments / observations have constrained these particles to be very light, of around 0.01eV. Also, they are expected to be very weakly interacting with conventional particles [15].
- **PBH**: This is the proposal that Primordial Black Holes - hypothetical kind of black holes created not from stellar collapse, but from heterogeneous density conditions in the early universe - are constituents of Dark Matter. In fact, they are a candidate liable to be the only constituent of DM, as, up to date, there is still a substantial window in parameter space that allows for it [5]. They have the particularity that they can be detected in a very specific way: through LIGO (and other gravitational wave experiments, current, and future ones). This is particularly interesting, as PHBs do not have the low mass range restricted as stellar Black Holes have, due to the different mechanism of formation. This means that the signal detected by LIGO (or any other) would be easily attributed

to a PBH. Also, these massive candidates could be studied by the very precise lensing techniques. For the moment, constraints coming from the observed stability of certain structures that coexist within DM halos give an upper bound for these candidates to be $5M_{\odot}$ [13]. The window which allows for PHBs to be the 100% of DM is $10^{17} < m_{PBH}/g < 10^{21}$ [16].

- **Millicharged:** This candidate was proposed in the context of trying to understand the anomalously large absorption in the Hydrogen 21cm signal measured at high redshift by the EDGES experiment [17]. This anomaly could only be explained in two ways, and both required new physics. One of them, the one interesting to us, explained the measurement as a signal of a new baryon-dark matter interaction which could have cooled the hydrogen beyond what one would expect from CMB measurements, via a scattering process. In general, *millicharged* DM particles are thought of as a sub-dominant contribution to the global composition of DM (see, for example, [18]). However, the candidate has not yet been ruled out, and it has some unique interest yet, as has been already stated. Besides, the sole fact that it is not ruled out yet is an encouragement for us to try and probe down the available parameter space, either to discover the particle, or to discard it definitively.

1.4 Objectives and structure of this project

Hereunder the overall outline of the project is presented, emphasizing its partial objectives and mentioning the theoretical background which is to be relevant in the analysis of the presented figures and results.

- In **Chapter 2**, the direct detection formalism applied to elastic spin-independent scattering is reviewed, as a proper understanding of this topic will ease our way into the subsequent chapters. The calculation of the differential event rate for generic DM particles and targets is gone through, and the necessary considerations regarding the speed distribution and density of the DM in the galactic halo are discussed. Also, the earth-scattering effect is introduced, and the relation between it and the time dependence of the detected signals is established. With the formalism at hand, the speed distribution at the detector as a function of the average incoming angle of DM flux is calculated, in order to set the base from which the recoil spectrum can be later computed.
- In **Chapter 3**, the differences between standard and *millicharged* DM models are exposed, and the formalism explained in **Chapter 2** is modified to adjust for the new type of particle. Once that this has been performed, the same calculations regarding the speed distribution at the detector are carried out, for later being able to compute the corresponding recoil spectrum.
- With the foundations fully developed, both scenarios (standard and *millicharged*) are compared via the time varying signals that both candidates would leave in different detectors in **Chapter 4**, and the differences between both of the scenarios are commented on. Based on this information, the best location for a detector to better distinguish between SI interacting DM and *millicharged* DM signals is proposed. Later, constraints on the mcDM particles are studied in order to conclude whether there is some parameter space which allows for the proposed experiment to be carried out.

It is worth remarking that the **novel approach** taken in this project is to use time modulation of the DM signal detected in underground or surface detectors, in order to try and distinguish

between the detection of a standard DM particle interacting predominantly in a Spin Independent fashion, and the detection of a *millicharged* DM particle, which has its unique form of interacting.

Throughout the text, examples will be given in order to understand the behaviour of different quantities related to DM direct detection. For these examples, we will mostly focus on two experiments: The CRESST 2017 surface run, carried out at the Max Planck Institute for Physics at Munich (MPI), and the CDMS-I, carried out at the Stanford Underground Facility (SUF), as suggested in [19].

The numerical code **verne** which has been used as the core to perform all the calculations and plots for this work, originally developed by B.J. Kavanagh, is made freely available online [here](#) [20]. It is worth noting, however, that all of the figures and general results that may be presented in this project, have been designed and performed by the student, via writing scripts which used some of the functions defined in **verne**. In some cases functions such as the one calculating the differential recoil rate were redefined by the student in order to fully understand not only the physics of the calculation, but also the inner workings of the code itself.

Chapter 2

Direct detection of Dark matter

Contents

2.1	Direct detection formalism	11
2.1.1	Derivation of the differential recoil rate, $\frac{dR}{dE_R}$	12
2.1.2	Derivation of the recoil energy	13
2.1.3	Spin-independent DM-nucleus differential cross section	14
2.1.4	Form factor correction	15
2.2	Understanding the DM Halo	17
2.2.1	Local DM density, ρ_0	17
2.2.2	Velocity distribution: Standard Halo Model (SHM)	17
2.2.3	SI recoil spectra for the Maxwellian distribution	18
2.2.4	Earth's motion and time dependence of the signal	20
2.3	Nuclear stopping of DM on Earth	22
2.3.1	Coordinate system	25
2.3.2	Velocity transfer	25
2.3.3	Speed distribution at the detector	27
2.4	Standard DM velocity distributions	28

In this chapter, a review on the basics of direct detection formalism is made, together with considerations regarding the speed distribution of DM in the galactic halo, the nuclear stopping of the DM particles in the Earth's nuclei, which attenuates the detected signal, and the time dependence of this signal. The examples that are going to be shown and discussed in this chapter are for standard SI interacting DM, in order to review the basics of the formalism to be introduced, and for the sake of later comparison with the *millicharged* scenario.

2.1 Direct detection formalism

Direct detection experiments aim to detect DM candidates by studying the recoil of the detector's nuclei when interacting with the flux of DM particles coming from the galactic halo, which the Earth is traversing - this can be seen as a static DM halo with the Earth moving through it with a certain speed, v_e . Here we will derive the expressions which will be relevant in the subsequent analysis.

2.1.1 Derivation of the differential recoil rate, $\frac{dR}{dE_R}$

The ideas guiding the following calculation have been extracted from Mark Thompson's Modern Particle Physics [21]. The calculation of the rate of interaction between particles starts by considering the incoming particle flux, defined as the number of particles crossing a unit area per unit time. Let ϕ_a be the incoming particle flux, traversing a region of space with n_b target particles per unit volume. The interaction rate per target particle, r_b , would be proportional to the incoming flux, ϕ_a , such that

$$r_b = \sigma \phi_a, \quad (2.1)$$

where σ is the proportionality constant, with units of area, which contains the physical information of the interaction, and represents the underlying quantum mechanical probability that a certain interaction will occur.

It is common to establish an analogy between this quantum mechanical parameter, σ , to the effective cross sectional area corresponding to each target particle. If the incoming particle crosses this tiny area around the target particle, they will interact. It has to be remembered that this is only an illustrative way of thinking about the problem, and should not be taken literally. With this picture in mind, the probability of interaction between incoming and target particles can be expressed as the ratio of the sum of all the effective cross sectional areas (Number of b particles in the region $\times \sigma$) to the total area, A , parametrizing the region of interest.

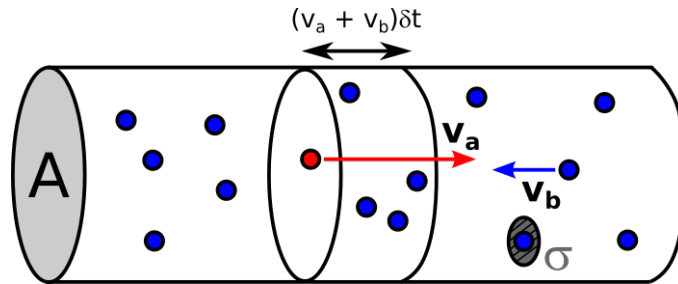


Figure 2.1. Illustration of a single particle of type a (velocity \mathbf{v}_a) crossing a region of space with b particles (velocity \mathbf{v}_b). A is the area parametrizing the region while σ is the effective cross-sectional area.

Let us fix our attention into an a particle, with velocity \mathbf{v}_a , traversing the region characterized by the area A , which contains the b particles, moving in the opposite direction as the former, with velocity \mathbf{v}_b (see fig. 2.1). In a differential time interval, δt , the a particle would cross a region containing

$$\delta N = n_b v A \delta t, \quad (2.2)$$

particles of type b , where $v = v_a + v_b$. Given the previous explanation, it is straightforward to see that the probability of interaction in that differential region of space is

$$\delta P = \frac{\sigma \delta N}{A}, \quad (2.3)$$

This can be further developed using Eq. (2.2) into

$$\delta P = \frac{\sigma n_b v A \delta t}{A} = \sigma n_b v \delta t. \quad (2.4)$$

Thus, we have

$$\frac{\delta P}{\delta t} = \sigma n_b v = r_a, \quad (2.5)$$

which, as shown in the right hand side of the equation, is precisely the rate of interaction per incoming a particle, r_a . Now, for a beam of a type particles with number density n_a confined within a volume V , the total rate of interaction, R , can be expressed as

$$R = r_a n_a V = (\sigma n_b v) n_a V = \sigma (n_a v) (n_b V) = \sigma \phi N_b. \quad (2.6)$$

That is,

$$R = \text{cross section} \times \text{flux} \times \text{total number of target particles}. \quad (2.7)$$

Taking this as the starting point, one can readily find the following to be true:

$$\frac{dR}{dE_R} = \phi \frac{d\sigma}{dE_R} N_b. \quad (2.8)$$

If one wants to take into account the speed distribution that the incoming particles had in the first place, the following 'weighted sum' shall be performed

$$\frac{dR}{dE_R} = \int_{v > v_{\min}} f(\mathbf{v}) \phi \frac{d\sigma}{dE_R} N_b d\mathbf{v}^3, \quad (2.9)$$

where the speed distribution would act as the weigh corresponding to each value of the velocity. The bounds of the integral are given by the minimum velocity that the incoming DM particle has to have in order to produce a recoil energy of value E_R . In later sections we will learn that there is also an upper bound to this integral, given by the maximum velocity that DM particles can have without escaping the gravitational influence of our galaxy. Remembering that $\phi = n_\chi v = \frac{\rho_\chi}{m_\chi} v$ (now, the particles are the incoming DM ones), and evaluating in 2.9, we have:

$$\frac{dR}{dE_R} = \frac{\rho_\chi}{m_\chi} \int_{v > v_{\min}} v f(\mathbf{v}) \frac{d\sigma}{dE_R} N_b d\mathbf{v}^3. \quad (2.10)$$

In order for the previous expression to be more general, one can express it in terms of number of interactions per unit detector mass, $m_N \cdot N_b$, instead of in terms of total number of interactions:

$$\frac{dR}{dE_R} = \frac{\rho_\chi}{m_\chi m_N} \int_{v > v_{\min}} v f(\mathbf{v}) \frac{d\sigma}{dE_R} d\mathbf{v}^3, \quad (2.11)$$

As can be deduced from Eq. (2.11), analysis carried out with this equation requires some previous assumptions regarding both parameters which are intrinsic to the candidate particles themselves, such as their mass and cross section of interaction with the nucleons; but also cosmological and dynamical parameters, such as their local density, ρ_0 , the galactic escape velocity or their speed distribution. Each assumption will be further developed and properly explained when examples are to be given.

2.1.2 Derivation of the recoil energy

It is now convenient to derive the expression of the recoil energy, E_R , so that, amongst other quantities, we can work out the lower limit of the velocity integral in equation Eq. (2.11). Consider a collision between a DM particle, of mass m_χ and velocity \mathbf{v}_χ and a target nucleus of mass m_N at rest in the laboratory frame. After the collision, the DM particle scatters elastically from the target nucleus with an angle θ^* in the center of mass frame (see figure 2.2).

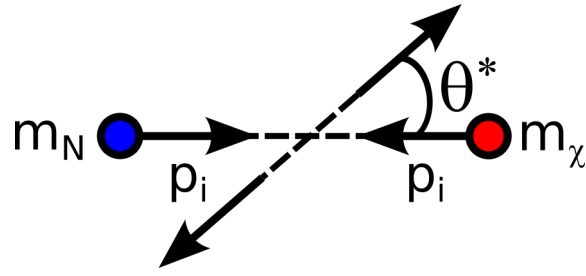


Figure 2.2. Two-body center of mass collision of an incoming DM particle with a target nucleus.

The center of mass velocity is given by

$$\mathbf{v}_{\text{CM}} = \frac{m_{\chi}}{m_{\chi} + m_N} \mathbf{v}_{\chi} = \frac{\mu_{\chi N}}{m_N} \mathbf{v}_{\chi}, \quad (2.12)$$

where we have defined

$$\mu_{\chi N} = \frac{m_{\chi} m_N}{m_{\chi} + m_N}. \quad (2.13)$$

After the collision, the velocity of the target nucleus (which was initially going at a velocity of v_{CM} in the CM frame) resolves into two components, one parallel to the line of movement before the collision, and one perpendicular to it. Thus, and returning to the lab frame, we have

$$\begin{cases} v_{N\text{lab}}^x = v_{\text{CM}} \cos(\theta^*) - v_{\text{CM}}, \\ v_{N\text{lab}}^y = v_{\text{CM}} \sin(\theta^*). \end{cases} \quad (2.14)$$

On the other hand, the kinetic energy transferred to the target nucleus in the lab frame is

$$\begin{aligned} E_R &= \frac{1}{2} m_N ((v_{N\text{lab}}^x)^2 + (v_{N\text{lab}}^y)^2) \\ &= \frac{1}{2} m_N v_{\text{CM}}^2 ((\cos(\theta^*) - 1)^2 + \sin^2(\theta^*)) \\ &= m_N v_{\text{CM}}^2 (1 - \cos(\theta^*)). \end{aligned} \quad (2.15)$$

Now, by evaluating Eq. (2.12) in E_R , we get:

$$E_R = \frac{\mu_{\chi N}^2 v_{\chi}^2 (1 - \cos(\theta^*))}{m_N} \quad (2.16)$$

Solving for v_{χ} in equation Eq. (2.16), it is clear that the minimum velocity that is able to produce a fixed recoil energy, E_R , corresponds to a head-on collision, when the scattering angle in the CM frame, θ^* , is equal to π . That is:

$$v_{\min} = \sqrt{\frac{E_R m_N}{2\mu^2}} \quad (2.17)$$

We have thus determined the lower bound of the velocity integral in Eq. (2.11).

2.1.3 Spin-independent DM-nucleus differential cross section

For the problem that we are tackling, spin independent (SI) scattering formalism is the appropriate framework to work on. To go deep into this formalism is beyond our scope, as it would require for us to calculate the interaction strength between the DM particles and the internal components of the nucleus in terms of the effective Lagrangian describing the interaction.

We can however safely make use of the following general expression for the spin-independent differential cross section [22, 23],

$$\frac{d\sigma}{dE_R} = \frac{m_N \sigma_p^{SI}}{2\mu_{\chi p}^2 v^2} A^2 F^2(E_R), \quad (2.18)$$

parametrised by σ_p^{SI} , the DM-proton cross section at zero momentum transfer. The A^2 factor (atomic mass of the target nucleus squared) responds to the SI interaction behaving coherently across the entire nucleus (reasonable for the range of momentum exchange of interest, not large enough to probe the inner structure of the nucleus) plus the assumption that the coupling of DM to both protons and neutrons is equal. The latter can be understood in terms of A scattering amplitudes, one for each scattering centre, all adding in phase [23]. $F^2(E_R)$ is the nuclear form factor, which takes the finite size of the nucleus into account. This will be further explained in the following sub-section.

2.1.4 Form factor correction

As previously mentioned, the form factor is introduced to take into account the finite size of the nucleus. When the momentum transfer is such that the corresponding wavelength is on the order of magnitude, or below, the nuclear radius, the probability of interaction or, better, the interaction cross section, falls with increasing recoil energy (larger momentum transfer equals larger recoil energy).

Within the First Born Approximation, the nuclear form factor is the Fourier Transform of a spherically symmetric mass distribution, normalized such that $F(0)$ is equal to 1 [24]:

$$\begin{aligned} F(q) &= \int \rho_{mass}(r) e^{i\mathbf{q}\cdot\mathbf{r}} d^3r = \int_0^{2\pi} d\phi \int_r^\infty r \rho_{mass}(r) \int_{-1}^{+1} e^{iqr\cos(\theta)} dr d(\cos(\theta)) \\ &= \frac{4\pi}{q} \int_0^\infty r \sin(qr) \rho_{mass}(r) dr. \end{aligned} \quad (2.19)$$

A problem arises here: the mass distribution in nuclei is hard to probe. To work around that, it is generally assumed that the distribution of mass in nuclei is approximately the same as that of its charge. However, instead of numerically integrating Eq. (2.19), most works use an already worked-out, analytical, form factor. Here, as in many other works, the Helm form factor [25], derived from combining the density of a uniform sphere with a Gaussian (which allows for the soft edges of the nuclei), will be used:

$$|F^{SI}(q)|^2 = \left(3 \frac{j_1(qr_n)}{qr_n} \right)^2 e^{-q^2 s^2}, \quad (2.20)$$

where

$$j_1(x) = \frac{\sin(x)}{x^2} - \frac{\cos(x)}{x} \quad (2.21)$$

is the spherical Bessel function. Both the effective nuclear radius r_n and the nuclear skin thickness s are fit parameters which are dependent on the target nucleus. In [23] Lewin and Smith performed a two-parameter least-squares fit to the Frick et. al compilation of muon spectroscopy data, to find that the value for r_n which best reproduced the Fourier transform of a two-parameter Fermi distribution was

$$r_n^2 = c^2 + \frac{7}{3} \pi^2 a^2 - 5s^2, \quad (2.22)$$

with

$$c = 1.23A^{1/3} - 0.60 \text{ fm.} \quad (2.23)$$

On their end, a and s are set to $a = 0.52 \text{ fm}$, and $s = 0.9 \text{ fm}$.

The behaviour of the form factor for different target nuclei can be seen in figure 2.3, where the maximum recoil energies that different mass DM particles can produce in the target nucleus are also shown, in order to get a glance at the lowest value that the form factor can take for a given scattering scenario. It can be seen that for light DM the effect of the form factor on the scattering cross section is little to none, but for heavier DM, the effect is more than apparent. This is because the momentum transfer between the heavy nuclei and a light particle is much less energetically efficient than the same process with a DM particle with a mass more similar to the nucleus'.

Also, it can be seen that the lighter the nucleus, the more momentum transfer (that is, the smaller the wavelength) is needed to lower substantially the value of F^2 , as expected. This can be better appreciated in figure 2.4, in which two nuclei with very different atomic masses are compared.

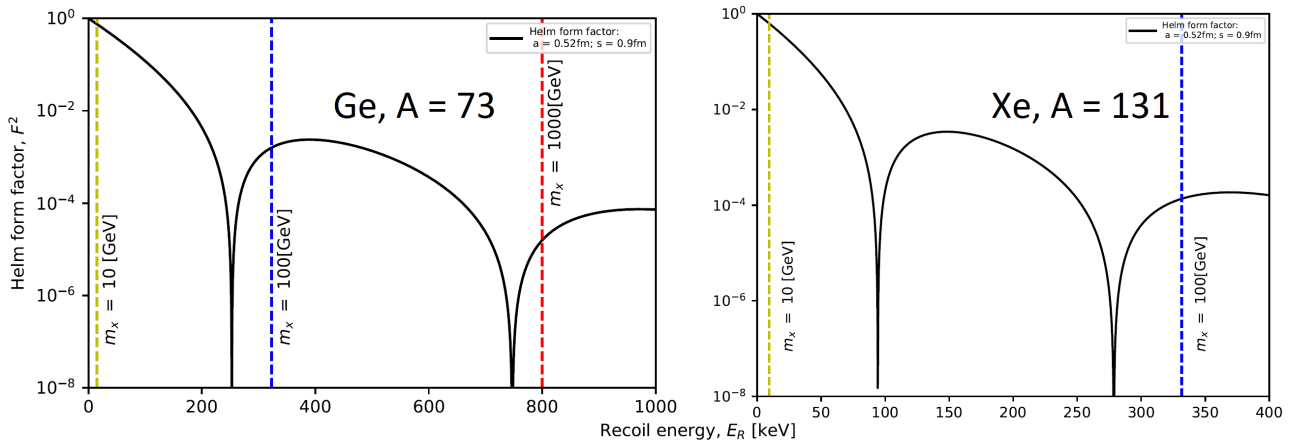


Figure 2.3. Helm form factor for Ge ($A = 73$, left) and Xe ($A = 131$, right). Note the change in the limits of the x-axis. Maximum recoil energies for different DM masses are shown as vertical lines.

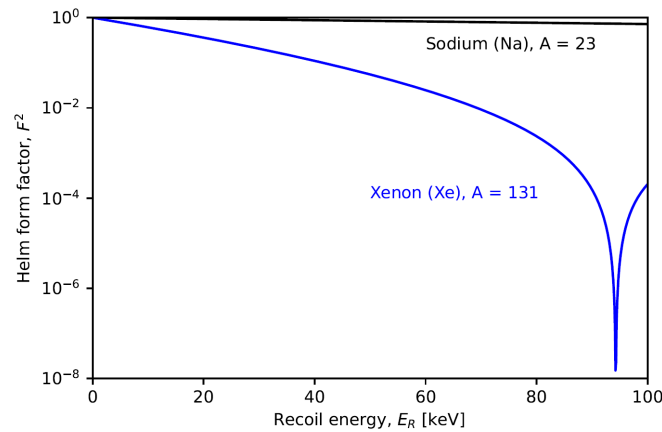


Figure 2.4. Low energy close up of the Helm form factor. Xe ($A=131$, blue) and Na ($A=23$, black)

The bumps and dips present in the form factor have to do with the internal structure of the nucleus, and respond to the diffraction pattern arising from the interference of the incoming wave with itself along the scattering event: constructive or destructive interference will happen depending on the 'size' of the wave or, equivalently, the magnitude of the momentum transfer, with respect to the nucleus it is interacting with.

In this kind of procedure is easy to overlook the fact that the resulting analytical form factor is of good use only after the parameters s and r_n have been fitted to a particular scattering data set, by using a very specific nuclear density model (two-parameter Fermi, in this case). In [24], Duda et. al discuss the limits of this kind of methodology, which can lead to substantial errors when high momentum transfers are to be expected. However, according to the referenced study, for the low mass regime in which we are interested in these errors are negligible, so we should be fine in using this model dependent Helm form factor, without worrying of it introducing large uncertainties. Note that in most cases, the form factor will be neglected in the calculations.

2.2 Understanding the DM Halo

2.2.1 Local DM density, ρ_0

The DM's local density parameter is usually calculated by first modelling the mass distribution of the Milky Way, and then adjusting ρ_0 until finding a range of values which are consistent with current MW's observational data, such as rotation curve measurements. Numerous works, using various observational data sets and including all kinds of MW models, some motivated by numerical simulations, agree that the local DM density lies in the $[0.2 - 0.4]$ GeV/cm³ range [26]. In most works, the benchmark value used is just $\rho_0 = 0.3[\text{GeV}/\text{cm}^3]$ and it is thus convenient to maintain the value, for the sake of cross checking.

2.2.2 Velocity distribution: Standard Halo Model (SHM)

At the moment, there are no direct measurements of the velocity distribution of DM in the MW, so it is usually derived from simulations. For the kind of work that we are doing, the standard way to proceed is to assume for the DM halo to be an isotropic and isothermal sphere with a density profile that falls with the square of the distance to its centre, $\rho(r) \propto r^{-2}$, and then solve the collisionless Boltzmann equation, thus finding the distribution $f(\mathbf{v})$.

This assumption is the **SHM, or standard halo model**, and it leads to a Maxwellian velocity distribution. The velocity dispersion, σ_v , corresponding to this distribution is related to the asymptotic value of the circular speed of objects orbiting the galactic centre, $v_c(r \rightarrow \infty) := v_c^\infty$ (at large radii the rotation curve of the SHM's isothermal sphere flattens, tending to the value v_c^∞), such that $\sigma_v = \sqrt{3/2}v_c^\infty$. Also, it is usually assumed that, at $r = R_0$, with R_0 being the Solar radius as measured from the Galactic centre, the circular speed $v_c(r = R_0) = v_c$ has already reached its asymptotic value, so that $v_c = v_c^\infty$ and, finally,

$$\sigma_v = \sqrt{\frac{3}{2}}v_c \quad (2.24)$$

Though not in general, in the standard halo model the most probable speed \bar{v}_0 and the circular speed are identical, and can be used interchangeably. In this work, the v_c parameter is fixed to be $v_c = 232\text{km/s}$, a reasonable value backed by experiments that rely on measurements of the solar velocity with respect to an object at rest with respect to the Galactic centre, or even by

experiments concerning direct measurements of local radial force [5].

Note that the aforementioned velocity distribution, $f(\mathbf{v})$, formally extends up to infinity, when, in reality, DM particles that exceed the Milky Way's escape velocity, $v_{esc}(r) = \sqrt{2|\Phi(r)|}$, with $\Phi(r)$ being the gravitational potential, will stop being gravitationally bound to it and, thus, are not interesting to direct detection experiments. For the subsequent analysis, we will use the value $v_{esc} = 544$ km/s [27].

This is usually dealt with by truncating the Maxwellian at some escape velocity, $v_{esc}(r = R_0)$, such that [28]:

$$\tilde{f}(\mathbf{v}) = \begin{cases} \frac{1}{N_{esc}} \left(\frac{3}{2\pi\sigma_v^2} \right)^{3/2} e^{-3\mathbf{v}^2/2\sigma_v^2}, & |\mathbf{v}| < v_{esc} \\ 0, & \text{otherwise} \end{cases} \quad (2.25)$$

where

$$N_{esc} = \text{erf}(z) - (2z/\sqrt{\pi})e^{-z^2} \quad (2.26)$$

is a normalization factor which becomes unity for an untruncated maxwellian ($v_{esc} \rightarrow \infty$). The parameter z is:

$$z = v_{esc}/\bar{v}_0,$$

and \bar{v}_0 is the most probable speed.

As ad hoc as this approach is, there are relatively recent hydrodynamical simulations of galaxy formation, including baryonic physics (which has a non-negligible impact on galactic DM distribution) which conclude that, at least in the solar neighbourhood, the SHM is a good fit for the actual distribution of galactic DM, and it can be used confidently when analysing direct detection experiments [29].

It has to be noted that the halo has a bulk motion relative to us, so that the distribution that we are interested in is not Eq. (2.25), but rather:

$$f(\mathbf{u}) = \tilde{f}(\mathbf{v}_{lab} + \mathbf{u}), \quad (2.27)$$

where \mathbf{u} is the velocity of the DM halo, and \mathbf{v}_{lab} is just the velocity of the observer on Earth with respect to the galactic rest frame.

2.2.3 SI recoil spectra for the Maxwellian distribution

Before continuing with the Earth's motion discussion, and now that we have already introduced most of the concepts required to calculate the desired recoil rate, it may be interesting to take a step back and discuss how does the differential recoil rate behave as a function of the DM particle's mass and target nuclei mass for the yet unperturbed (as it has not interacted with Earth nuclei for the moment) Maxwellian distribution. This way, we can ease later discussions regarding the behaviour of this quantity in the Earth-scattering scenario.

For this preliminary analysis we need some specific information, particularly the **DM mass**, m_x and the corresponding value of the **SI DM-nucleon cross section**. For this matter, it is important to have in mind which pairs of values are compatible, and have not yet been excluded by other experiments or other studies.

For light DM we shall use the recent study from E. Aprile et. al, [30], in which they probe the parameter space of light dark matter by studying the conventional elastic scattering scenario while adding the the irreducible inelastic processes that also occur along the scattering events, such as the Migdal effect or the Bremsstrahlung effect. In particular, they give updated limits to the DM-nucleon cross section as a function of the mass of the particle, see figure 2.5.

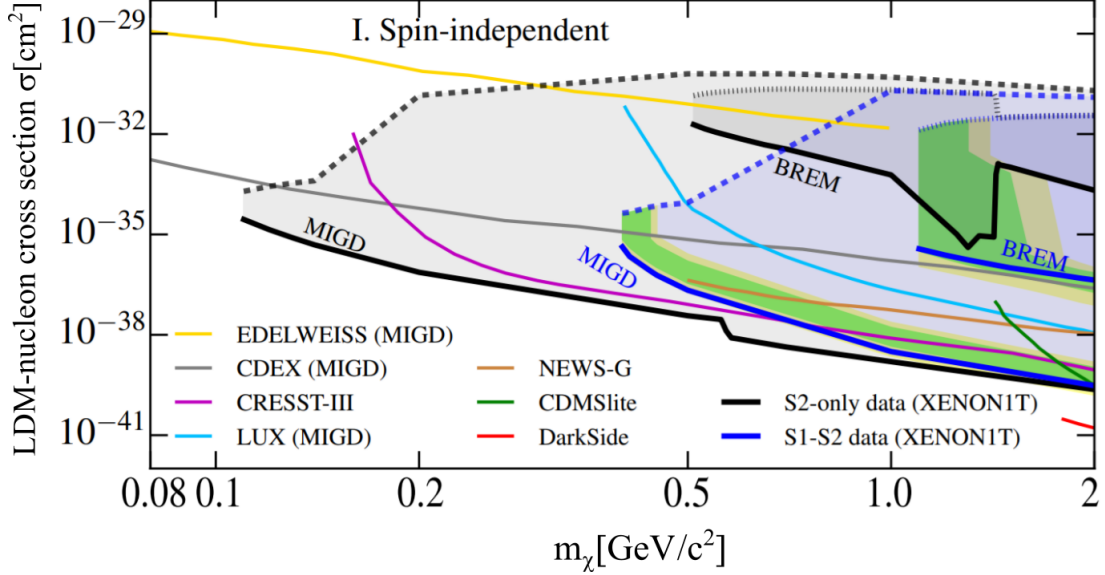
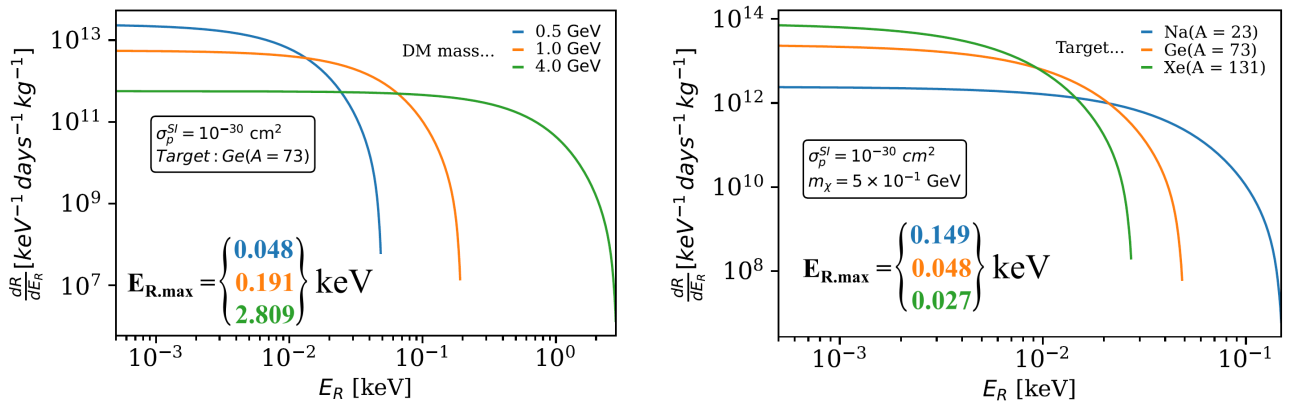


Figure 2.5. Limits on the SI DM-nucleon interaction cross-sections at 90% C.L. Signal models from both Migdal and Bremsstrahlung effects in the XENON1T experiment have been used. Adapted from Ref. [30].

From the figure, we can see that for light DM we are safe to use $\sigma_p \approx 10^{-30}$ for our examples.

Now we will proceed on to examine the dependence of the differential recoil rate arising from the Maxwellian distribution of velocities, Eq. (2.25), on the DM mass and on the target nuclei mass.

Note again that we are not taking into account the Earth stopping effect and, because of that, we just simply integrate the Maxwellian distribution over all angles (in a spherical fashion), and use it to perform the calculation of Eq. (2.11).



(a) Fixed target (Germanium) + variable mass.

(b) Fixed mass (0.5 GeV) + variable target.

Figure 2.6. Example plots for the recoil spectrum of the unperturbed Maxwellian distribution describing the DM halo. A log-log plot has been for the spectra to be seen nicely. In both plots, the maximum recoil energy corresponding to each curve is indicated with the appropriate color.

The calculations of the differential recoil rate for both fixed target / fixed DM mass scenarios are plotted in figure 2.6.

The first thing to be noticed in the left panel is that the maximum value of the recoil rate is larger the smaller the DM mass, which has to do with the $1/m_\chi$ factor in Eq. (2.11) and the $1/\mu_{\chi p}^2$ factor in Eq. (2.18).

In the right panel, we can see that the maximum recoil rates are reached for the heaviest target nuclei, which has to do with the A^2 factor in Eq. (2.18).

Apart from these rather trivial scaling factors, we also note that the rate at which dR/dE_R falls is different for different DM masses (or different target nuclei masses in the right panel). If we neglect the form factor, we can see that this dependence of how quickly does the differential recoil rate falls with m_χ and m_N does not come directly from the differential cross section or any pre-factor but it actually comes from the velocity integral in 2.11. Note that the integral is performed for velocities greater than a certain v_{\min} . The thing is that v_{\min} depends on m_χ and m_N (see Eq. 2.17), so that, for example, if we were to fix the target and then choose a light DM particle, the factor multiplying the E_R inside the square root becomes large, thus making v_{\min} grow quickly with growing E_R . This in turn necessarily means that the integral in 2.11 must decrease, as the integration enclosure is also decreasing - remember that at some point, the velocity distribution is very small, as it tends to 0 with increasing speeds. A similar explanation can be given when considering the variation with μ_N , but the other way around: the larger the target nucleus, the quicker the decline of the differential recoil rate. Both of these effects can be clearly seen in figure 2.6.

We shall expect a similar behaviour later on, when Earth-scattering is introduced - of course, we would expect smaller recoil rates, due to the attenuation caused by the DM-nucleon scattering.

2.2.4 Earth's motion and time dependence of the signal

Due to the motion of the Local Standard of Rest (v_{LSR}), the Sun's peculiar velocity ($v_{\odot,pec}$), the motion of the Earth around the Sun (v_{\oplus}), and the daily revolution of the Earth ($v_{\oplus,rot}$), a time dependence arises from \mathbf{v}_{lab} in equation Eq. (2.27).

In **section 2.3** we will study how does the interaction of the DM with the Earth's nuclei modify the velocity distribution along the path which the DM particles traverse in their way to the detector. What is important for now is that the modification to the original velocity distribution depends on the path taken by the DM particles or, in other words, it depends on the position of the detector with respect to the average direction of the incoming DM flux. It is therefore useful to define an angle γ , which is defined as the angle between the direction of the mean DM flux coming from the Halo, and the position vector of the detector on Earth:

$$\gamma = \cos^{-1}(\langle \hat{\mathbf{v}}_\chi \rangle \cdot \hat{\mathbf{r}}_{\text{det}}). \quad (2.28)$$

Here, the mean DM velocity is given by

$$\langle \hat{\mathbf{v}}_\chi \rangle = -\mathbf{v}_{lab}(t). \quad (2.29)$$

Note that the time dependence in \mathbf{v}_{lab} is transferred on to the angle γ , which will be important later when discussing the annual modulation of the detected DM signal.

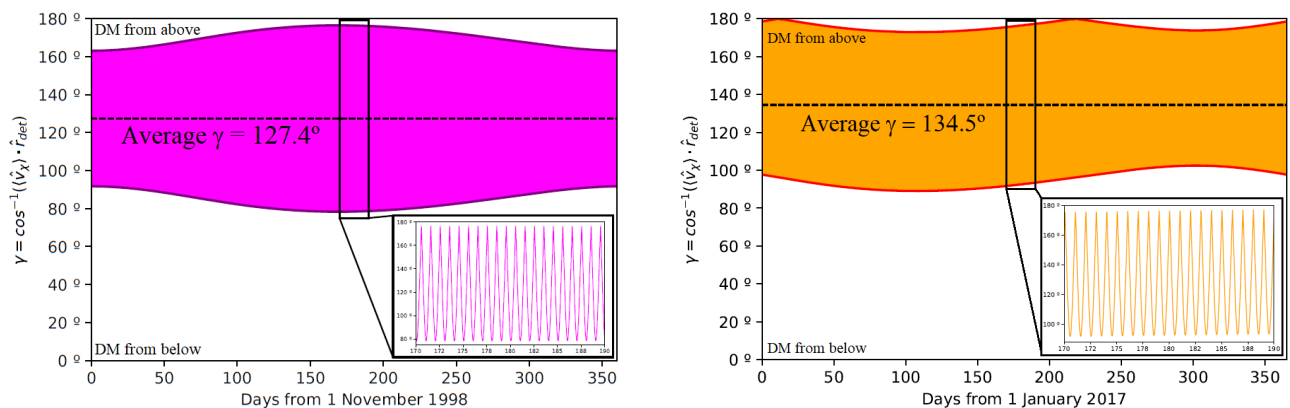
For the calculation of the dot product in γ , we need to precisely know the components of the vector quantity v_{lab} . For that, we need to be able to transform between the galactic rest frame and the detector rest frame. This calculation is rather tedious, and it is not included in this project, but it is performed with great detail in [31]. The calculation is performed within the VERNE environment by the LABFUNCS module, which outputs \mathbf{v}_{lab} in the laboratory frame coordinates, $\mathbf{v}_{lab} = (v_{NS}, v_{WE}, v_Z)$, where the first component is the velocity in the North-South axis, the second is that in the West-East axis, and the last one is the velocity along the axis perpendicular to the surface of the Earth, pointing up through the floor.

The quantities used for this calculation have been chosen to be (in km/s, and in the galactic frame of coordinates):

$$\begin{cases} \mathbf{v}_{\odot, \text{pec}} = [11.1, 12.2, 7.3] \\ \mathbf{v}_{\text{LSR}} = [0, 220, 0] \end{cases}$$

while the orbital speed of the Earth has been set to $v_{\oplus} = 29.8 \text{ km/s}$.

For our purposes, the selection of the time window to work on is rather arbitrary, so, in order to see the behaviour of $\gamma(t)$ we simply follow the suggestion in [19] of plotting γ in the one year window that spans the CDMS-I experiment's exposure [32], carried out at the Stanford Underground Facility (SUF, latitude = 37.4°N , longitude = 122.2°W), see figure 2.7a. We also plot the angle γ for the Max-Planck Institute for Physics (MPI, latitude = 48.1°N , longitude = 11.57°E) in a one year span throughout 2017, covering the CRESST 2017 surface run [33], in order to see how the change in the localization of the detector affects the modulation, see figure 2.7b.



(a) One year span covering the **CDMS-I** experiment, carried out at Stanford Underground Facility (SUF).

(b) One year span covering the **CRESST 2017** experiment, operated at the M.P. Institute (MPI).

Figure 2.7. Average direction of DM flux versus time. The darker envelope function shows the extreme values of γ , while the small variation due to Earth rotation is shown in the zoomed subplot.

In both cases, the slow modulation coming from the Earth's translation motion (darker envelopes in 2.7) and the faster modulation coming from the daily rotation of the Earth are shown. Even though the shape of the modulation is visibly different, note that the average γ over the course of one year is very similar in both cases, around 50° away from the vertical, which means that, for both MPI and SUF, the average DM particle will not have to traverse large path lengths interacting with nuclei, as the particle would not need to cross the entire Earth before reaching the detectors, which means that the signal is not too suppressed when detected. The small daily variation is identical in both scenarios aside from the overall modulation amplitude and the phase of the oscillation, both differences due to the different locations

of the detectors.

In the following sections we will study how DM interacts with nuclei on the Earth and how this affects the initial velocity distribution along the collision path. Then, we will study how do these scattering-modified distributions depend on the angles describing the incoming DM trajectory (particularly, how they depend on γ), so that we can finally calculate the speed distribution of DM particles at the detector, accounting for all possible trajectories.

2.3 Nuclear stopping of DM on Earth

Ultimately, our goal is to determine the velocity distribution of the particles at a given detector, as this will give us the detected signal by calculating the corresponding recoil rate. This means that we first need to understand the way in which the DM particles interact with all the nuclei in their way, and then understand how this behaviour depends on the particular trajectory of the incoming particles. The approach and ideas used here follow those taken in [19]. In the cited paper, the developed formalism encompasses two assumptions:

- Very heavy DM, of about 10^5 GeV.
- Strongly interacting DM - large cross sections.

The first assumption ensures that the angle of deflection of the DM particles in the scattering process is small, while the second one guarantees that the number of scattering events that the DM particle undergoes is large. Both of these facts allow us to approximate the DM trajectories within the Earth (plus atmosphere and detector) as straight lines, an approximation necessary to ascertain some of the equations that follow this discussion.

However, and as we have already justified in the introduction, we are interested in the low mass regime. At first, this may seem like a problem if this formalism is to be used but, in [34] (particularly, figure 5) it is shown, by comparison with full and more careful Monte Carlo simulations, that the formalism in [19] (the one discussed below) is also valid for small DM masses - down to a few GeV.

With this background, and holding on to the continuous scattering assumption, we can write the rate of change of the mean energy of colliding DM particles as

$$\frac{d\langle E_\chi \rangle}{dt} = - \sum_i n_i(\mathbf{r}) \langle E_R \rangle_i \sigma_{i\chi}(v) v, \quad (2.30)$$

where $n_i(\mathbf{r})$ is the number density of nuclei of species i at a distance \mathbf{r} , $\sigma_{i\chi}(v)$ is the total DM-nucleus scattering cross section, while v is the velocity of the DM particles.

The term $\langle E_R \rangle_i$ is the average recoil energy transferred on to the nuclei of species i by the elastic collision with DM particles. It can be written as

$$\langle E_R \rangle_i = \frac{1}{\sigma_{i\chi}(v)} \int_0^{E_{R,i}^{max}} E_R \left(\frac{d\sigma_i}{dE_R} \right) dE_R \quad (2.31)$$

The upper bound in Eq. (2.31) is the maximum possible recoil energy that can be transferred to the nucleus of species i from a collision with an incoming DM particle. This quantity can

be readily deduced from Eq. (2.16) by evaluating the θ^* that ensures the maximum possible value of the RHS of the equation, which of course is $\theta^* = \pi$ (head-on collision), thus getting

$$E_{R,i}^{max} = \frac{2\mu_{\chi i}^2 v^2}{m_i}. \quad (2.32)$$

Note that we are indexing nuclear species in i , so this subindex will be used interchangeably with the previously used subindex N . Now, by combining Eq. (2.18) with Eq. (2.31) we get

$$\langle E_R \rangle_i = \frac{1}{\sigma_{i\chi}(v)} \int_0^{E_{R,i}^{max}} E_R \left(\frac{m_i \sigma_p^{SI}}{2\mu_{\chi p}^2 v^2} A_i^2 F_i^2(E_R) \right) dE_R \quad (2.33)$$

It is convenient here to perform a change of variables, in favour of exposing the full dependence of $\langle E_R \rangle$ on relevant quantities. We change from E_R (which goes from 0 to $E_{R,i}^{max}$) to $x E_{R,i}^{max}$, with x ranging from 0 to 1. This gives

$$\begin{aligned} \langle E_R \rangle_i &= \frac{1}{\sigma_{i\chi}(v)} \int_0^1 x (E_{R,i}^{max})^2 \left(\frac{m_i \sigma_p^{SI}}{2\mu_{\chi p}^2 v^2} A_i^2 F_i^2(x E_{R,i}^{max}) \right) dx \\ &= \frac{1}{\sigma_{i\chi}(v)} \int_0^1 x \left(\frac{2\mu_{\chi i}^2 v^2}{m_i} \right)^2 \left(\frac{m_i \sigma_p^{SI}}{2\mu_{\chi p}^2 v^2} A_i^2 F_i^2(x E_{R,i}^{max}) \right) dx \\ &= \frac{\mu_{\chi i}^4 v^2}{\mu_{\chi p}^2 m_i \sigma_{i\chi}(v)} \frac{\sigma_p^{SI}}{A_i^2} \int_0^1 (2x) F_i^2(x E_{R,i}^{max}) dx \\ &= \frac{\mu_{\chi i}^4 v^2}{\mu_{\chi p}^2 m_i \sigma_{i\chi}(v)} \frac{\sigma_p^{SI}}{A_i^2} C_i(m_\chi, v), \end{aligned} \quad (2.34)$$

where we have identified the integral on the third line with $C_i(m_\chi, v)$, which from now on will be referred to as the coherence factor.

This coherence factor accounts for the suppression of the mean recoil energy emerging from the form factor, F_i^2 , and it is normalized such that for a point-like scattering centre $C_i = 1$. From the already discussed behaviour of the form factor, we expect to see increasing suppression of the mean recoil energy for heavy DM particles with increasing speed, as we have illustrated in figure 2.8. For large DM masses, we can see that at almost every significant velocity the coherence factor is fairly suppressed, whereas we can see that for lighter DM, it takes a really high velocity for the coherence factor to fall just a little. In fact, we can see that, for the maximum possible velocity that a DM particle can have before escaping the gravitational pull of the Galaxy (that is, $v_{esc} + v_{lab} \approx (544 + 220)\text{km/s} \approx 770\text{km/s}$), the coherence factor only falls a 16%. On top of that, particles with such large speeds do not even have a large weight in the speed distribution describing the DM halo (see Eq. (2.25)), so substantial suppression of the interaction probability coming from C_i should not at all be expected for light DM, which encourages us to neglect C_i for the rest of the calculations.

We can evaluate now Eq. (2.34) in Eq. (2.30), so that:

$$\frac{d\langle E_\chi \rangle}{dt} = -\frac{v^3}{m_\chi \mu_{\chi p}^2} \sigma_p^{SI} \sum_i n_i(\mathbf{r}) \frac{\mu_{\chi i}^4}{m_i} A_i^2 C_i(m_\chi, v). \quad (2.35)$$

where the coherence factor is not dropped, for completeness.

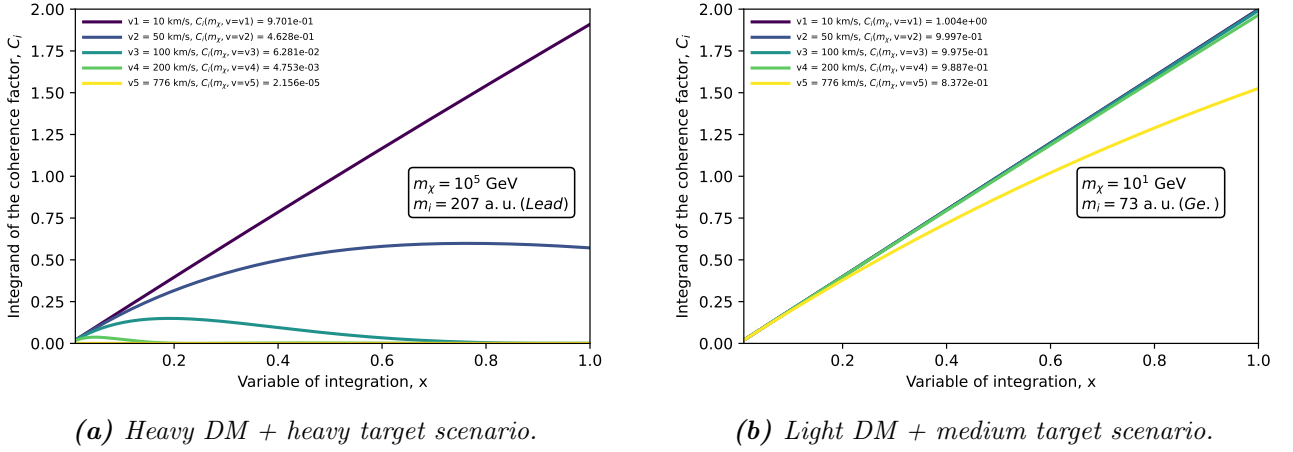


Figure 2.8. Coherence factor integrand as a function of the recoil energy. Each curve represents a different DM velocity value, which is indicated in the top left corner of the figure, alongside the value of the corresponding coherence factor $C_i(m_\chi, v)$.

It is now interesting to see how does the velocity of the DM particle change along the straight line distance, D , which it has to travel through. By a simple change of variables we have:

$$\frac{dv}{dD} = \frac{dv}{dt} \frac{dt}{dD} = \frac{dv}{dE_\chi} \frac{dE_\chi}{dt} \frac{dt}{dD}.$$

If now we evaluate $E_\chi = m_\chi v^2/2$, we have that

$$\frac{dv}{dD} = \frac{1}{v^2} \frac{dE_\chi}{dt}, \quad (2.36)$$

which readily yields:

$$\frac{dv}{dD} = -\frac{v}{m_\chi \mu_{\chi p}^2} \sigma_p^{SI} \sum_i n_i(\mathbf{r}) \frac{\mu_{\chi i}^4}{m_i} A_i^2 C_i(m_\chi, v), \quad (2.37)$$

where D is the distance travelled by the DM particle in a straight line.

With Eq. (2.37) we are able to know how the velocity of the DM particle changes over a straight-line path traversing the Earth, its atmosphere and the detector's shielding, provided that we know the density profiles of the different elements that form them. As we are using `verne`, we shall use the same elements contemplated within the code, and the same data sets. The three regions that the particles have to traverse are, thus,

- Atmosphere: Straight line from top of the atmosphere to surface of the Earth. Two elements are included, Oxygen and Nitrogen, and their atmospheric density profiles are taken from the ISO's (International Standard Organization) standard atmosphere [35].
- Earth: Straight line from surface of the Earth to detector's shielding. In `verne`, 8 elements are included - oxygen (O), silicon (Si), magnesium (Mg), iron (Fe), calcium (Ca), sodium (Na), sulfur (S) and aluminium (Al). Density profiles are taken from the tabulated data in [36].
- Detector's shielding: Both in the atmosphere and Earth, the straight line path involved some dependence on the angle of incidence of the soon to be detected DM particle. However, for the thin detector shieldings we take a fixed path length, which of course depends on the chosen detector.

2.3.1 Coordinate system

It is now convenient to introduce the coordinate system used throughout the rest of the text, as specific expressions for the path length and the radial distance in terms of angular coordinates are needed in order to calculate relevant quantities. The system can be visualized in figure 2.9.

If we now define $R_E = 6371\text{km}$ as the radius of the Earth and $h_A = 80\text{km}$ as the height of the atmosphere, then we can write the straight line path length from the top of the atmosphere to the detector as:

$$l = r_{det}\cos(\theta) + \sqrt{(R_E + h_A)^2 - (r_{det}\sin(\theta))^2} \quad (2.38)$$

With this we can write the radial distance from the Earth's centre to a particle which has travelled a distance D along the straight line trajectory as:

$$r = \sqrt{(R_E + h_A)^2 + D^2 + 2D(r_{det}\cos(\theta) - l)} \quad (2.39)$$

In particular, these expressions are needed in order to integrate Eq. (2.37), as will become evident in the next subsection.

Remember that the angle θ refers to the trajectory of an individual particle, while γ refers to the mean direction in which all the DM particles are coming to the Earth. Note also that the radial distance is needed in order to calculate the density profiles, $n_i(\mathbf{r})$.

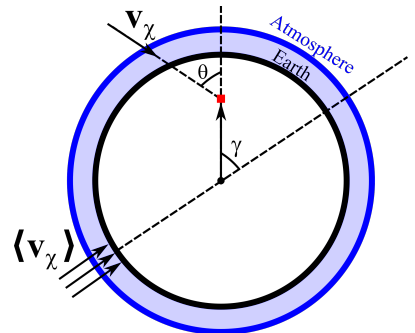


Figure 2.9. Coordinate system used to describe the trajectory of a DM particle, \mathbf{v}_χ , and of the mean average flux of DM $\langle \mathbf{v}_\chi \rangle = -\mathbf{v}_{lab}$.

2.3.2 Velocity transfer

With both Eq. (2.38) and Eq. (2.39) we are able to integrate Eq. (2.37) such that

$$v_f = v_i + \int_0^l \frac{dv}{dD}(v, r)dD, \quad (2.40)$$

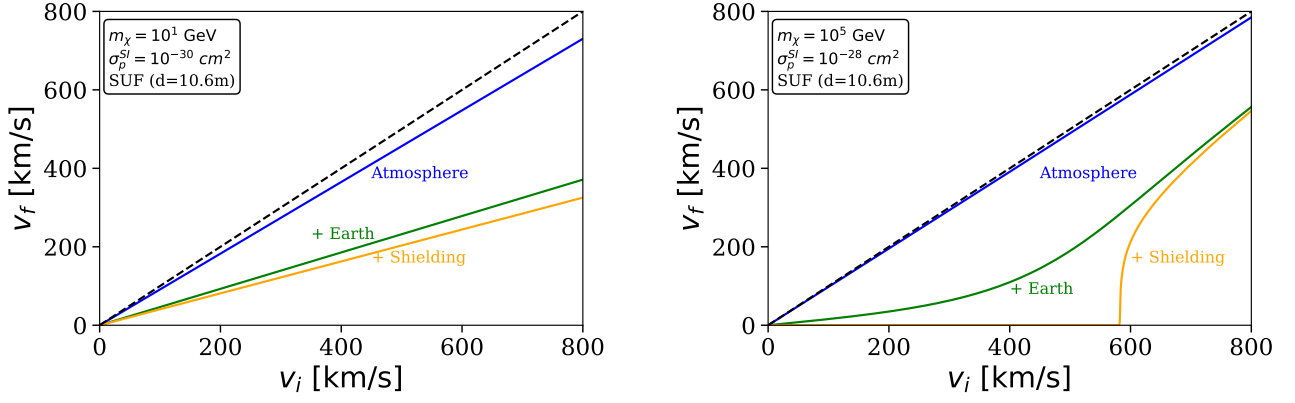
which is the first step into getting the speed distribution at the detector (see next section). Note that the integration of Eq. (2.37) has to be performed numerically through an ODE solver, as required by the non trivial dependence of dv/dD on r and v .

With equation Eq. (2.40) we can study the velocity transfer that happens to the incoming DM particles right from the initial state on the top of the atmosphere up to the final state, on the detector, for a given DM trajectory.

For the following example, the incoming individual DM trajectory will be such that $\theta = \pi$ - that is, particle coming from overhead.

In the case of light DM (see 2.10a), where we can neglect the coherence factor, it can be seen from Eq. (2.37) (evaluating $C_i = 1$) that by integrating Eq. (2.40) we obtain final speeds which follow a proportionality relationship such that $v_f \propto v_i$, a behaviour which can be seen in the left panel of figure 2.10.

Note that the SUF location has been chosen to show the behaviour of the velocity transfer process because it is sufficiently buried underground ($depth = 10.6m$) so that the stopping effect is clearly seen in the **Atmosphere** to **Atmosphere+Earth** transition. Had we used MPI



(a) Light DM + smaller DM-nucleus cross section.

(b) Heavy DM + larger DM-nucleus cross section.

Figure 2.10. Example plots of the velocity transfer for DM particles coming directly from overhead and being detected at SUF. Each curve represents the final velocity of the DM particles after going through the corresponding layer.

($d = 0.3\text{m}$) as an example (while maintaining the other parameters), the difference between the **Atmosphere** and the + **Earth** curves would have been negligible, and the stopping effect would not have been that apparent. Also, note that the SI cross section has been set to be somewhat small, so that the particles are not fully stopped in the atmosphere or early in the Earth.

Given that the chosen cross section is rather small in both cases, we expect the atmosphere to have the least effect on the velocity of the incoming particles, as can be readily seen from the blue lines in 2.10a and 2.10b. The thick layer of Earth that DM has to go through clearly has a more notable slowing effect, while the shield only slows a little more the incoming DM particles in the light DM scenario.

In order to give a broader understanding of the velocity transfer process, the example of a heavy DM particle traversing the same three phases (atmosphere, Earth, detector's shielding) is also given, in 2.10b, even if this project is focused on light DM. Here, we can see a number of effects. First, the cross section has been set to be two orders of magnitude higher than in the left panel, in order to account for the low efficiency of heavy particles in transferring kinetic energy - if the cross section is as small as in the other case, the velocities of the DM particles would not be largely affected by the scattering process, and the plot would not be of much interest.

We can see again that the atmosphere has not too much effect on the incoming velocities, due to the not too large cross section. However, in the Earth and shielding regimes we see a different behaviour than the expected one in a light DM case. Where we would expect a linear behaviour with $C_i = 1$ we now see that at large speeds the particles are less and less stopped, a fact that emerges from the suppression of the SI cross section at large momentum transfers, as shown on figure 2.4. In particular, we see that slow particles are completely stopped once that they have gone through the detector's shielding, and that only fast moving particles survive, again, because of the coherence factor - had we neglected C_i , even the fast particles would have been stopped, and so no particle could have been detected in the underground experiment. It is important to remember that the explanation given here for the coherence factor is just an illustration, and we will proceed to neglect it in our relevant calculations later on, due to our focus on light DM.

2.3.3 Speed distribution at the detector

Provided that we know the initial distribution of velocities, $f(\mathbf{v}_i)$, which in this case we assume it is a Maxwellian as the one presented in Eq. (2.25), it is easy to go from $\tilde{f}(\mathbf{v}_i)$ to $\bar{f}(\mathbf{v}_f)$ - the distribution of velocities at the detector, after the particles go through the scattering process - by a simple change of variables:

$$f(\mathbf{v}_i)d^3\mathbf{v}_i = \bar{f}(\mathbf{v}_f)d^3\mathbf{v}_f \quad (2.41)$$

Here we will again rely on the straight-line formalism, such that $\hat{\mathbf{v}}_i = \hat{\mathbf{v}}_f := \hat{\mathbf{v}}$. Thus, if we write Eq. (2.41) in terms of the corresponding unit vectors:

$$\begin{aligned} f(\mathbf{v}_i)v_i^2 dv_i d\hat{\mathbf{v}}_i &= \bar{f}(\mathbf{v}_f)v_f^2 dv_f d\hat{\mathbf{v}}_f \\ \Rightarrow \bar{f}(\mathbf{v}_f) &= f(\mathbf{v}_i) \left(\frac{v_i}{v_f} \right)^2 \frac{dv_i}{dv_f}. \end{aligned} \quad (2.42)$$

Now, as we are not interested in directional detection, we must integrate $\bar{f}(\mathbf{v}_f)$ over all incoming angles and, for that, we need to understand how \mathbf{v} in Eq. (2.25) depends on the angular coordinates shown in figure 2.9.

For that, let \mathbf{v} be the velocity of a DM particle in the galactic rest frame, \mathbf{v}_χ the velocity of a DM particle in the Earth's frame and \mathbf{v}_{lab} the velocity of the lab (Earth) with respect to the DM halo (galaxy). They are related by:

$$\mathbf{v} = \mathbf{v}_\chi - \mathbf{v}_{lab} \quad (2.43)$$

Squaring both sides of the equation, we have:

$$|\mathbf{v}|^2 = \mathbf{v}_\chi^2 + \mathbf{v}_{lab}^2 - 2v_\chi v_{lab} \cos(\alpha) \quad (2.44)$$

With α being the angle between the velocity of a particular DM particle and the velocity of the Earth. Looking at figure 2.9, we can relate this angle to both θ and γ , as well as to ϕ , the azimuthal angle (not shown on figure 2.9), such that:

$$\cos(\alpha) = \sin(\gamma)\sin(\theta)\cos(\phi) + \cos(\gamma)\cos(\theta). \quad (2.45)$$

It is from the previous equation that the velocity dispersion gets the dependence on γ and, thus, on time.

Now that the form of the velocity dispersion in terms of (γ, θ, ϕ) has been fully determined, the integral over all angles can be performed. First, we have:

$$\bar{f}(v_f) = \int v_f^2 \bar{f}(\mathbf{v}_f) d^2\hat{\mathbf{v}} = \int f(\mathbf{v}_i) v_i^2 \frac{dv_i}{dv_f} d^2\hat{\mathbf{v}} \quad (2.46)$$

Note that we have distinguished between $f(\mathbf{v})$, the velocity ($\mathbf{v} = (v_x, v_y, v_z)$) distribution and $f(v)$, the speed ($v = |\mathbf{v}|$) distribution, and we have used the following relation: $f(v) = \int v^2 f(\mathbf{v}) d^2\hat{\mathbf{v}}$.

Here, we are treating v_i as the initial velocity needed to obtain a given final velocity in the detector for a particle which is travelling in a straight line defined by the direction $\hat{\mathbf{v}}$. Now, changing to the angular integrals, we have:

$$\begin{aligned} \bar{f}(v_f, \gamma(t)) &= \int f(\mathbf{v}_i, \gamma(t), \phi, \theta) v_i^2 \frac{dv_i}{dv_f} d\cos(\theta) d\phi \\ &= \int_{-1}^{+1} \left[\int_0^{2\pi} f(\mathbf{v}_i, \gamma(t), \phi, \theta) d\phi \right] v_i^2 \frac{dv_i}{dv_f} d\cos(\theta), \end{aligned} \quad (2.47)$$

where we have used that the only ϕ dependence arises in the $f(\mathbf{v}_i)$ function, from Eq. (2.45) - not in v_i or in dv_i/dv_f , as can be readily seen from figure 2.9.

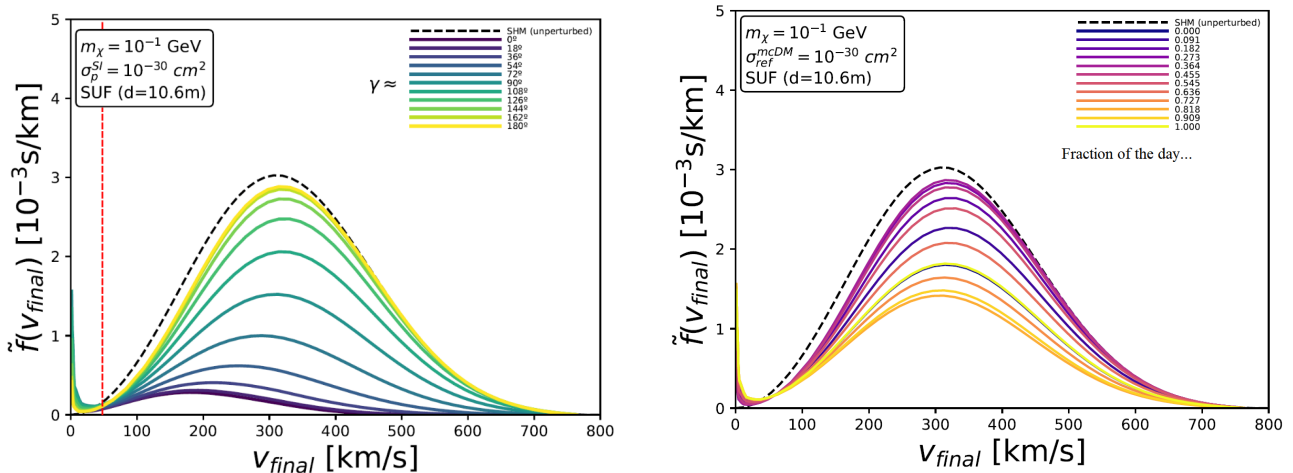
Note that this integral needs to be performed numerically, owing to the integral in Eq. 2.40 (which we need to solve in order to perform the numerical derivative dv_i/dv_f), which cannot be solved analytically because of the dependence of dv/dD on the DM velocity.

2.4 Standard DM velocity distributions

With all the formalism at hand, we can discuss the way in which the Earth stopping process affects the initial DM velocity distribution, as a function of the mean DM flux. Then, we can study the dependence of the recoil spectra on time, which will ultimately give us the corresponding signal.

As the signals will be further explained and compared in a separate chapter, we will just focus here in explaining the behaviour of the velocity distributions for a particular scattering scenario.

In order to put forward specific examples, we will focus here on the SUF (CDMS-I) experiment. In figure 2.11a, various speed distributions at the SUF detector for given values of the DM mass, the DM-nucleon cross section and the angle γ are shown.



(a) Final velocity distribution as a function of γ , with evenly spaced γ values.

(b) Final velocity distribution as a function of time, one curve every 2h.

Figure 2.11. Final speed distribution at SUF. Final speed distribution of light DM particles at the stanfordd Underground Facility (SUF), after propagating through the atmosphere, Earth and Pb shielding. The dashed curve is the unperturbed Maxwellian speed distribution. The distribution is shown as a function of evenly spaced values of the average DM flux, γ . Velocities below the dashed vertical line are not able to produce a 10keV recoil, which is the threshold corresponding to CDMS-I.

In particular, the distribution for 11 different values of γ is presented, from 0° - average DM particles directly coming from below, larger path to reach the detector - to 180° - average DM particles directly coming from overhead, shorter path to reach detector. In the right panel (2.11b) we have calculated the distribution of velocities for a set of γ values corresponding to 12 time stamps distributed evenly throughout one arbitrary day - remember that we can calculate the angle γ for any time value that we want, through Eq. (2.28). The latter will be the set of curves used to calculate the time dependence of the differential and total recoil rates

later on, in **Chapter 4**.

Note that γ denotes the average direction of the incoming DM, so that even for $\gamma = 0^\circ$, there is not a total suppression of the population of particles arriving at the detector, as can be seen from the dark blue curve in 2.11a.

Also note, looking at figure 2.11b, that gamma (which grows down-up) does not escalate linearly with time. Instead, it follows the dependence shown on figure 2.12, a calculation which has been performed in the same manner as the ones in 2.7.

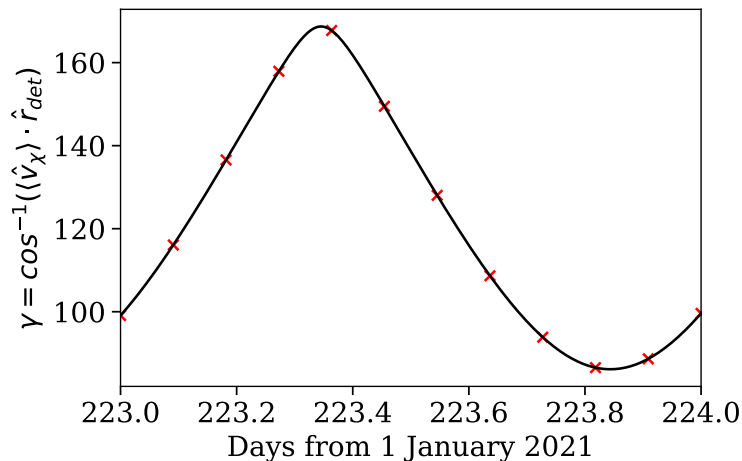


Figure 2.12. *Daily variation of γ . The time stamps and corresponding gamma values used to plot figure 2.11b are marked with crosses.*

We can also see that the peaks of the distributions in 4.1 shift to the right for increasing γ . This is due to the fact that, even though the initial Maxwellian distribution is isotropic in the Galactic rest-frame, it is anisotropic in the Earth's reference frame. This means that, for us, particles travelling parallel to the **mean** DM flux are the ones with larger velocities, while the ones travelling anti-parallel to the DM flux are the slower ones. For example, for $\gamma = 0^\circ$, particles that travel with large velocities must also cross most of the Earth until reaching the detector, meaning that the large speeds region in the corresponding distribution (dark blue curve in 2.11a) is not very populated, as most of those particles have been attenuated before reaching it. On the other hand, slower particles would come mostly from above, having to cross less portion of the Earth and thus mostly surviving until reaching the detector. The situation is the other way around for $\gamma = \pi$, so that the curves in between just transition smoothly from one scenario to the other - that is, from a lower peak velocity to a higher one - thus the right-hand shift.

Now that we are aware of the behaviour of these distributions, the next step would be to compute the recoil rates corresponding to the γ curves of interest, in order to make apparent the time dependence of dR/dE_R . However, this is going to be performed in **Chapter 4**, in which the signals of both standard DM and Millicharged DM are going to be compared and analyzed.

Chapter 3

Direct detection of *Millicharged* Dark Matter

Contents

3.1	An overview on the candidate	30
3.1.1	<i>Millicharged</i> DM-nucleus differential cross section	30
3.2	<i>Millicharged</i> recoil spectra for the Maxwellian distribution	32
3.3	Nuclear stopping of <i>millicharged</i> DM on Earth	33
3.3.1	Velocity transfer	34
3.4	<i>Millicharged</i> DM velocity distributions	35

In this chapter, the formalism that has been gone through in **Chapter 2** is adapted to the *millicharge* DM particles scenario, so that the velocity distributions at a given detector can be calculated, setting up the foundations for the comparison and analysis which is going to be done on **Chapter 4**. It has to be noted that the functional forms of the recoil rate and recoil energy extracted in **Chapter 2**, along with the considerations made for the velocity distribution associated to the DM halo and the motion of the Earth are all valid here. The differentiating quantity is the DM-nucleus interaction cross section, and it is this difference, and the unique effects that come with it, what is going to be discussed in this chapter.

3.1 An overview on the candidate

We have to be aware that the current project does not aim to fully develop or study the specific theoretical framework in which *millicharged* DM is contemplated. We will now mention it briefly, but our focus is essentially the functional form of the differential cross section describing the interaction of our candidate particle with the nuclei on Earth (and atmosphere and detector), such that calculations similar to those performed in **Chapter 2** with Spin Independent, electrically neutral, DM particles can also be done here.

From the Lagrangian describing the *millicharged* DM model, a coupling between the DM field and the SM photon arises. As a consequence, the former obtains an electric *millicharge*, ϵ [37].

3.1.1 *Millicharged* DM-nucleus differential cross section

The aforementioned coupling introduces a Coulomb-like interaction between our DM candidate and electrically charged particles within the SM.

Now, the DM-nucleus differential cross section, which is the one that's interesting to us, given the problem at hand, is:

$$\frac{d\sigma_N^{mcDM}}{dE_R} = \frac{2\pi Z_N^2 \varepsilon^2 \alpha^2}{m_N v^2 E_R^2} F^2(E_R), \quad (3.1)$$

where Z_N and m_N are the charge number and the atomic mass of the nucleus N, respectively, ε is the *millicharge* (in units of the electron charge) and α is the SM dimensionless fine structure constant ($\alpha \approx 1/137$). The form factor appearing in Eq. (3.1) is the same form factor discussed in **section 2.1.4**.

It is worth noting that the continuous and almost straight line trajectories formalism still holds true here, and it is enhanced even, due to the $1/E_R^2$ dependence of the cross section. If we take a look at the expression for the recoil energy, we note that E_R becomes smaller as the scattering angle decreases; and a smaller recoil energy means a higher cross section or, better, a higher scattering probability. In conclusion, *millicharged* DM is more likely to scatter in the forward direction, which further justifies the 'straight line' scattering formalism described throughout **section 2.4**.

It is also common to talk about the total cross section, which is obtained from integrating equation Eq. (3.1). For this, an important effect, specific for this kind of interaction, has to be introduced first: the **screening effect**. If the incoming *millicharged* DM particles are traveling at sufficiently low speeds, the momentum transfer with the interacting nucleus will not be large enough for the particle to probe the inside of the target, which means that the electron cloud of the nucleus screens its charge, so that the DM particle will see it as a neutral scattering centre, nullifying the electrical interaction and, thus, making the scattering probability drop to zero. Particularly, we can identify this transition with the instant in which the momentum transfer between the DM particle and the nucleus becomes comparable to the typical momentum of the electron, αm_e . Converting from the momentum to a recoil energy, we have the expression for the screening recoil energy,

$$E_R^{screen} = \frac{(\alpha m_e)^2}{2m_N} \quad (3.2)$$

Now, for us to find the expression of the screening velocity, we shall match the screening energy with the maximum possible recoil energy. That way, we obtain the largest value for the velocity for which this screening effect arises,

$$\frac{(\alpha m_e)^2}{2m_N} = \frac{2\mu_{\chi N}^2 v_{screen}^2}{m_N} \Rightarrow v_{screen} = \sqrt{\frac{(\alpha m_e)^2 m_N}{4\mu_{\chi N}^2 m_N}} = \frac{\alpha m_e}{2\mu_{\chi N}}. \quad (3.3)$$

Here, $m_e \approx 0.511\text{MeV}$ is the mass of the electron and $m\mu_{\chi N}$ is the reduced mass of the DM-nucleus system. Below this velocity, the screening effect becomes apparent, and the corresponding DM particles will not be perturbed by Earth-scattering effects.

Having this effect in mind, we can integrate Eq. (3.1) to obtain:

$$\begin{aligned} \sigma_N^{mcDM}(v) &= \int_{E_R^{screen}}^{E_R^{max}} \frac{d\sigma_N^{mcDM}}{dE_R} dE_R = \frac{2\pi Z_N^2 \varepsilon^2 \alpha^2}{m_N v^2} \int_{E_R^{screen}}^{E_R^{max}} \frac{dE_R}{E_R^2} \\ &= \frac{2\pi Z_N^2 \varepsilon^2 \alpha^2}{m_N v^2} \left[\frac{1}{E_R^{screen}} - \frac{1}{E_R^{max}} \right] = \frac{2\pi Z_N^2 \varepsilon^2 \alpha^2}{m_N v^2} \left[\frac{2m_N}{\alpha^2 m_e^2} - \frac{m_N}{2\mu_{\chi N}^2 v^2} \right] \\ &= \frac{4\pi Z_N^2 \varepsilon^2 \alpha^2}{v^2} \left[\frac{1}{\alpha^2 m_e^2} - \frac{1}{4\mu_{\chi N}^2 v^2} \right], \end{aligned} \quad (3.4)$$

which is manifestly velocity dependent. Note that the form factor has been neglected here because in Coulomb-like interactions the momentum transfer is typically rather small [37]. The fact that we are focusing on light DM of course backs this decision.

This dependence of the total cross section on the velocity prevents us from defining a total cross section in the same way as we can in the SI case, so we define a 'reference' cross section, σ_{ref}^{mcDM} , as the value of the DM-proton cross section evaluated at an arbitrary velocity, $v_{ref} = \sqrt{2m_e\alpha/2\mu_{\chi N}}$, such that:

$$\sigma_{ref}^{mcDM} = \frac{4\pi\epsilon^2\mu_{\chi N}^2}{m_e^4\alpha^2} \quad (3.5)$$

This quantity will serve us later, in **Chapter 4** when trying to compare the SI model with the *millicharged* one. Also, the code VERNE is prepared in such a way that whenever σ_p^{SI} were to be used internally in the SI scenario, the value for σ_{ref}^{mcDM} is used instead, if the *millicharged* interaction is the one being studied.

3.2 *Millicharged* recoil spectra for the Maxwellian distribution

Our goal here is to calculate the recoil spectrum without taking into account the Earth-scattering effect for the *millicharged* interaction, for some particular values of the **DM mass**, the **milli-charge** ϵ and the **effective cross-section**. For a reason that will become clear in the next sub-section, we set $m_\chi = 5\text{GeV}$. For later comparison with the SI case, it may be interesting to match the value of the SI DM-proton cross section with the *millicharged* reference cross section defined in Eq. (3.5). For the moment, we could set this value to be $\sigma_{ref}^{mcDM} = 1 \cdot 10^{-30} \text{cm}^2$, which converts back to $\epsilon = 3.5 \cdot 10^{-11}$ (in units of the electron charge). According to [5], for this DM mass, the maximum milli-charge that one can have is $\epsilon_{max} = 3.5 \cdot 10^{-7} (m_\chi = 5[\text{GeV}])^{0.58} = 8.9 \cdot 10^{-7}$, so our value for ϵ seems safe enough. In Chapter 4, we will discuss whether these parameters are reasonable within the current *millicharged* paradigm.

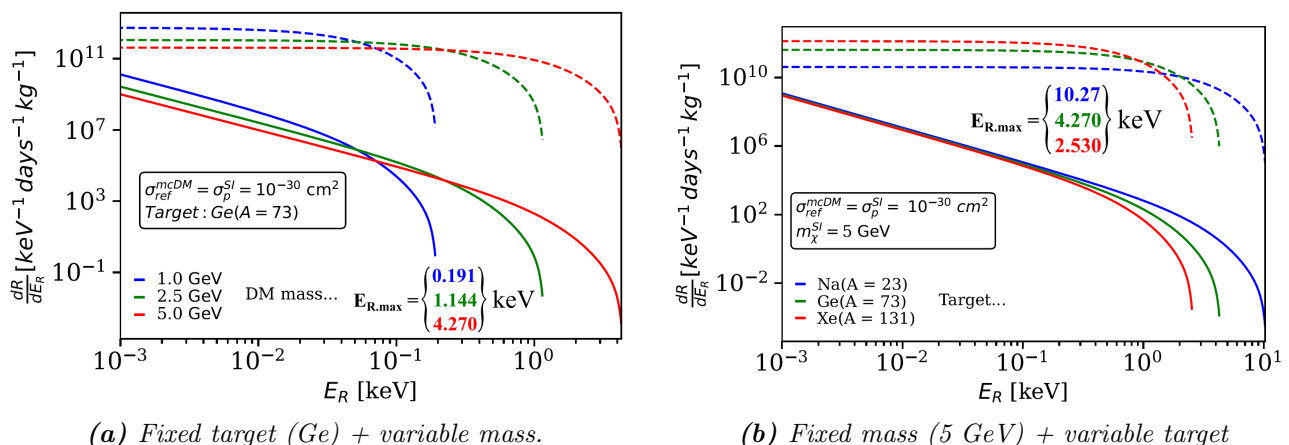


Figure 3.1. Example plot for the *millicharged* (solid line) recoil spectrum of the unperturbed Maxwellian distribution describing the DM halo. A log-log plot has been used for the spectra to be seen nicely. In both plots, the maximum recoil energy corresponding to each curve is indicated with the appropriate color. The recoil spectra for SI interacting DM particles are also plotted (dashed line), for the same DM mass.

We can now plot the recoil spectra for various DM masses with a fixed target, see figure 3.1. Note that each curve will also have a unique ε value, in order to preserve the value of the reference cross section.

We can see that the behaviour is fairly similar to that discussed in section 2.2.3 for the case of SI, at least in what has to do with the maximum values of the recoil rates. However, we can see that the differential recoil rate falls with increasing recoil energy a lot faster for the *millicharge* interaction, which is ascribable to the dependence of the *millicharge* differential cross section on $1/E_R^2$. Of course, in a linear plot, the exponentially decaying behaviour becomes apparent. Also, note that the order of magnitude of the recoil rates is rather similar for both the *millicharge* and SI interactions, which is mostly due to the fact that the SI DM-proton cross section has been matched with the effective cross section.

3.3 Nuclear stopping of *millicharged* DM on Earth

Here we will go through the same kind of calculations as in section 2.3, but now taking into account the corresponding form of the differential cross section, as well as the aforementioned screening effect.

Following the already explained approach (see equations Eq. (2.30) and Eq. (2.31)), we write the average recoil energy transferred from the DM particle to the target nucleus as:

$$\begin{aligned}\sigma_N^{mcDM} \langle E_R \rangle_i &= \int_{E_{R,i}^{screen}}^{E_{R,i}^{max}} E_R \left(\frac{2\pi Z_i^2 \varepsilon^2 \alpha^2}{m_i v^2 E_R^2} F^2(E_R) \right) dE_R \\ &= \frac{2\pi Z_i^2 \varepsilon^2 \alpha^2}{m_i} \int_{E_{R,i}^{screen}}^{E_{R,i}^{max}} \frac{1}{E_R v^2} F^2(E_R) dE_R\end{aligned}\quad (3.6)$$

Now, changing variables such that:

$$(E_R) \rightarrow (xE_R^{max}), \quad x \in [0, 1]$$

we have

$$\sigma_N^{mcDM} \langle E_R \rangle_i = \frac{2\pi Z_i^2 \varepsilon^2 \alpha^2}{v^2 m_i} \int_{\left(\frac{\alpha m_e}{2\mu v}\right)^2}^1 \left[\frac{F^2(xE_{R,i}^{max})}{x} \right] dx \quad (3.7)$$

As we know, we are going to be dealing with light DM particles, so it is not that important here to analyze the coherence factor that would arise for this kind of interaction. Thus, we make $F^2(xE_{R,i}^{max})$ tend to one and then solve the integral analytically, such that:

$$\sigma_N^{mcDM} \langle E_R \rangle_i = \frac{4\pi Z_i^2 \varepsilon^2 \alpha^2}{v^2 m_i} \log \left(\frac{2\mu v}{\alpha m_e} \right). \quad (3.8)$$

Now, combining Eq. (3.7) with Eq. (2.30), we have that:

$$\frac{d\langle E_\chi \rangle}{dt} = - \sum_i n_i(\mathbf{r}) \frac{4\pi Z_i^2 \varepsilon^2 \alpha^2}{v m_i} \log \left(\frac{2\mu v}{\alpha m_e} \right), \quad (3.9)$$

which, if we change variables as we did in Eq. 2.36, transforms into

$$\frac{dv}{dD} = - \frac{4\pi \varepsilon^2 \alpha^2}{v^3} \sum_i n_i(\mathbf{r}) \frac{Z_i^2}{m_i} \log \left(\frac{2\mu v}{\alpha m_e} \right). \quad (3.10)$$

Now, and in a similar manner as in the SI case, Eq. (3.10) gives us the necessary information to know how the *millicharged* particles traverse the different media until reaching the detector. The three layers to be considered are, naturally, the same (atmosphere, Earth and detector's shielding) but, this time, the charge numbers of the different components are needed in order to perform calculations.

3.3.1 Velocity transfer

Of course, the coordinate system is the same as the one described in **section 2.3.1**, and the relationship between the initial velocity at the top of the atmosphere, v_i , and the final velocity at the detector, v_f is still Eq. (2.40).

Therefore, we can calculate the velocity transfer in the scattering process of *millicharged* particles. Given that, as it has already been stated, in this Coulomb-like interactions the momentum transfer is not large in general, we need to use a sufficiently heavy DM particle in order to clearly see the effect of the attenuation due to the interaction with nuclei on Earth. It has been found that a mass of about $m_\chi \sim 5\text{GeV}$ is able to give us some interesting enough curves. We also need to decide beforehand the value for the effective cross section, which, for the moment, is set to be $\sigma_{ref}^{mcDM} = 10^{-30}\text{cm}^2$, and also the specific trajectory of DM particles, which is set to be $\theta = \pi/2$.

What we obtain is the plot shown in figure 3.2.

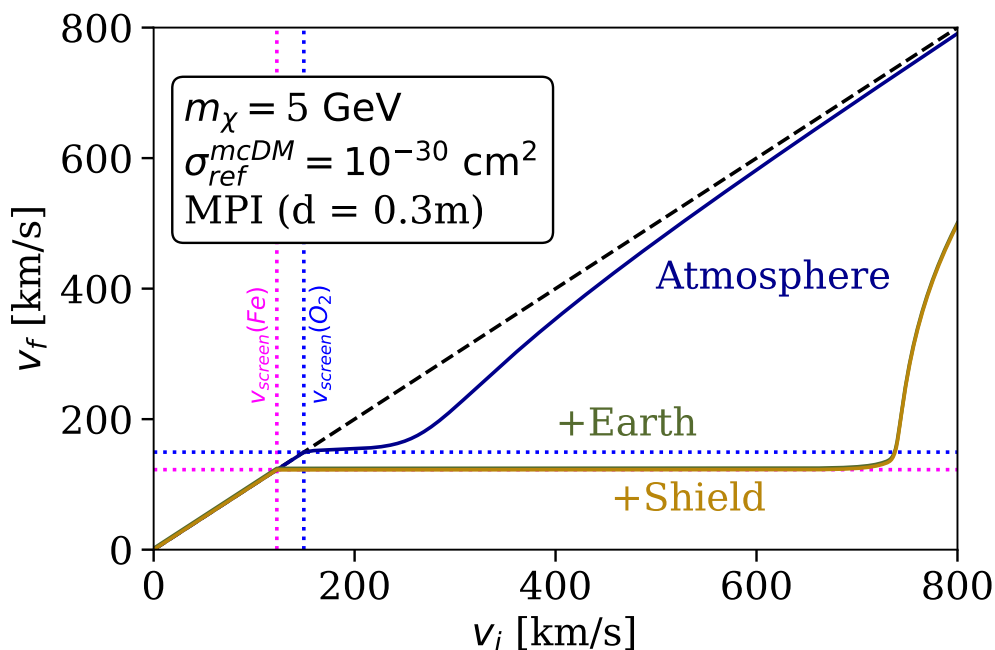


Figure 3.2. Example plot of the velocity transfer for millicharged DM particles ($\epsilon = 3.5 \cdot 10^{-11}$) coming with an angle $\theta = \pi/2$ and being detected at MPI. Each curve represents the final velocity of the DM particles after going through the corresponding layer.

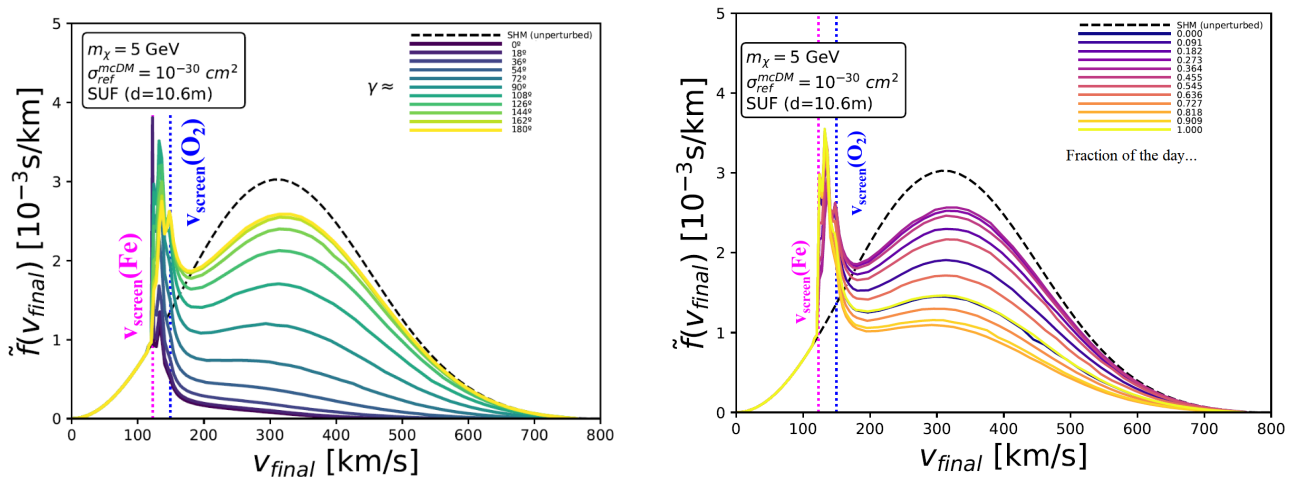
We can readily see a few different effects already. First, we can see that the initial velocities are not at all modified in the first $\sim 120\text{km/s}$, which is due to the already explained screening effect: Particles with speeds low enough will 'see' nuclei as electrically neutral objects, therefore not interacting at all with them, as the interaction with which we are dealing is a coulombic one. The value of the speed at which velocities begin to be modified in the 'Atmosphere' curve matches the screening velocity corresponding to Oxygen, which makes perfect sense, as this is the heaviest nucleus considered within this layer. In the '+Earth' curve, that value matches

the screening velocity corresponding to iron, the heaviest nucleus considered within Earth (and thus the lowest v_{screen} for Earth scattering).

From v_{screen} on, we see that the velocities are in fact modified by the scattering effect. Particularly, the fact that the total DM-nucleus cross section depends on the DM velocity is very apparent. By looking at the functional form of the total cross section (Eq. (3.4)), we can see that, for small enough speeds (but greater than v_{screen}), the term in brackets enhances σ_N^{mcDM} due to the $-1/v^2$ term inside it. The closer the speed to $v_{screen}(O_2)$, the greater the enhancing effect. However, the $1/v^2$ term in the prefactor quickly takes over the expression for large speeds, suppressing the probability of interaction at high v , thus making v_f tend to the original velocities (dashed curve). A similar discussion can be done for the two remaining curves, bearing in mind that the subtracting term in Eq. (3.4) has a $\mu_{\chi N}^2$ in the denominator, which means that the 'enhancing' of the cross section is more persistent, and thus the curves begin to tend to v_i much later in the x-axis, but much more abruptly. Note that the curves for the Earth and shielding are almost identical. This is because the particles with speeds above $v_{screen}(Fe)$ have already been slowed down to almost the v_{screen} of the detector's material (Cu in the case of MPI), making both curves be almost the same. For larger velocities, which are not slowed down to $v_{screen}(Cu)$, the cross section is already very suppressed, so that the shielding effect on the velocities is also really small.

3.4 Millicharged DM velocity distributions

Now, we are finally able to plot the velocity distributions for *millicharged* particles, as a function of the mean DM flux (and, therefore, time), same as in figures 4.1. The example plots are calculated for the SUF (CDMS-I) experiment here as well.



(a) Final velocity distribution of millicharged particles as a function of γ , with evenly spaced γ values.

(b) Final velocity distribution of millicharged particles as a function of time, one curve every 2h.

Figure 3.3. Final speed distribution at SUF. Final speed distribution of moderate-mass millicharge DM particles at the Stanford Underground Facility (SUF), after propagating through the atmosphere, Earth and Pb shielding. The dashed curve is the unperturbed Maxwellian speed distribution. The distribution is shown as a function of evenly spaced values of the average DM flux, γ .

The basic discussion regarding the behaviour of the velocity distribution has already been made in section 2.4, around figure 4.1, so it isn't necessary to go through it all over again.

However, there are some very visual differences (apart from the different time dependence, which will be studied in the next Chapter) with the plots on figure 4.1, and they have all to do with the screening effect explained in **section 3.1.1**. First, we can see that velocities below the screening velocity of the largest nucleus on Earth (Iron, Fe) - thus the lowest screening velocity considered - are not at all affected by the Earth-stopping effect. Again, this has to do with our charged DM particles 'seeing' the nuclei on Earth as neutral objects, with which they do not interact. The high-speed region of the plots seems rather similar to that of the SI distributions, but where we do see a difference is in the region just above v_{screen} . Particles in that region seem to be piling up, and that is because, at that point, they have been slowed so much, that they are losing energy very slowly, thus facilitating this 'bunching' effect. The peaks that we see in that region correspond to the screening velocities for the different materials considered. In the plots, only the lowest value of v_{screen} for both the atmosphere and the Earth layers are shown.

Also, there is another even more subtle effect playing out, and that is the fact that, precisely at v_{screen} , our formalism breaks, as the interaction probability quickly drops to zero. To save the normalization of the velocity distributions, we could add by hand a population of particles with the form of a Dirac's delta distribution at $v = v_{screen}$.

However, this is quite complicated to perform, and given that the velocities at which this effect happens are low enough, we might not need to worry about it when calculating the recoil spectrum, as will be shown in **Chapter 4**.

Chapter 4

Signal analysis. Constraints and proposed detectors

Contents

4.1	Time-dependence of the differential recoil rate	37
4.2	Time-varying SI and <i>millicharge</i> signals	38
4.2.1	Signals for various detectors and analysis	39
4.3	Constraints	41

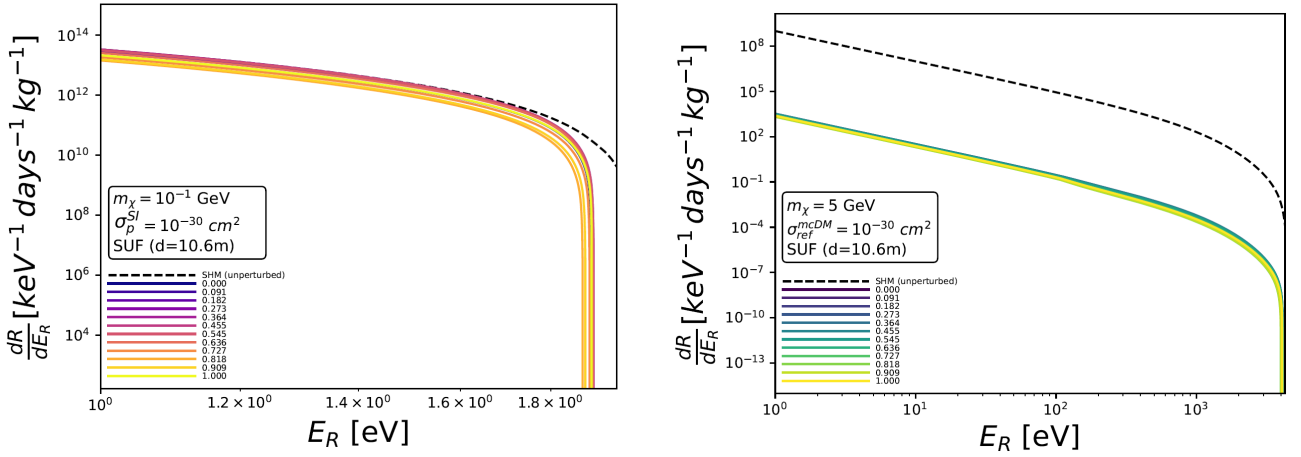
In this chapter, the time dependence of the differential recoil rates for the distributions shown in figures 2.11b and 4.1b is shown, so as comment on their apparent differences. Then, the time dependence of the total recoil rate for various detector locations and depths are calculated for both SI and *millicharge* DM, thus obtaining two DM signals for each detector. The differences between the signals are studied, and some final comments are given regarding the best location for a future detector of DM which could distinguish between both of these signals. Finally, the parameter space of *millicharge* DM is explored, so as to check whether the interesting parameters of *millicharged* DM discussed throughout this section have not yet been excluded.

4.1 Time-dependence of the differential recoil rate

As we have been advancing throughout the text, in what follows the differential recoil rate as a function of time is presented for both SI and *millicharge* interacting DM particles, with the set of parameters corresponding to those on figures 2.11b and 4.1b.

Note that these two are **example** plots, and they are not necessarily going to be used to extract meaningful information regarding the detected time-varying signal. This is done specifically in the next sub-section for several location of the detectors, and several depths.

Nevertheless, we can already see that the information gathered from the recoil rates for the Maxwellian distribution, discussed in **sections 2.2.3** and **3.2** did lead to a nice understanding on the functional form of the differential recoil rates, both of them follow approximately the same behaviour discussed in the mentioned sections. For example, in figure 4.1a we can see that both the form of the curves and their corresponding maximum value match closely with the light blue curve in figure 2.6a, which is the one with the adequate value of the DM mass. The same can be said from the right panel, except from the fact that the curves after the Earth-scattering have been prominently attenuated.



(a) Differential recoil rate for SI interacting DM particles, as detected at SUF.

(b) Differential recoil rate for millicharged interacting DM particles, as detected at SUF.

Figure 4.1. Example plots of the differential recoil rate at SUF for various time-stamps throughout the 11th of August of 2021. Each curve is plotted for a unique value of time and, therefore, a corresponding value of $\gamma(t)$.

The time dependence is not very apparent in this kind of plots, as the curves are all very close together. The way to really see this dependence is by extracting the total recoil rate for each curve,

$$R_{tot} = \int_{E_{R,th}}^{E_R^{max}} \frac{dR}{dE_R} dE_R, \quad (4.1)$$

where $E_{R,th}$ is some threshold energy corresponding to the particular detector which is being used ; and plot these values as a function of the time stamps for which each curve has been calculated. This is precisely the calculation that is going to be performed in the next subsection, for a fixed mass and spin independent DM-proton cross section (effective cross section in the case of mcDM) and different choices of detectors, for which two parameters are going to be played around with: the depth of the detector, and its latitude, essentially. This will give us information on whether the time dependence of both signals is different enough so that it can give a possible signature in one detector over any other.

4.2 Time-varying SI and millicharge signals

In order to ensure a great deal of Earth-scattering effect involved (essential to the time varying aspect of the signal), the value of the probing mass has been set to be $m_\chi = 5\text{GeV}$. We are still in the low-mass regime, but we also ensure that *millicharged* DM leaves an interesting signal, same as in figure 3.2. The value for the cross section has been set to be $\sigma_p^{SI} = \sigma_{ref}^{mcDM} = 1 \cdot 10^{-30}\text{cm}^2$, for consistency with the rest of the text.

For the detectors, three latitudes have been selected:

- lat = 45 °N ; long = 122.2 °W
- lat = 0 ° ; long = 122.2 °W
- lat = 45 °S ; long = 122.2 °W

The longitudes have been set arbitrarily, given that they have little effect in the time dependence, as can be seen in figure 2.7. In order for the signals to be better compared later, we just

use the same longitude for all of the three detectors.

In what comes to depths, the northern detector has been selected to also be experimented with, with different depths. Particularly, 1m and 10m.

4.2.1 Signals for various detectors and analysis

Hereunder we will include both the obtained signals with a brief comment on what we are seeing. We will use the following amplitude parameter in order to compare the figures:

$$A = \frac{R_{max} - R_{min}}{\bar{R}} \quad (4.2)$$

with \bar{R} being the average rate, depicted in the plots as a blue dashed line.

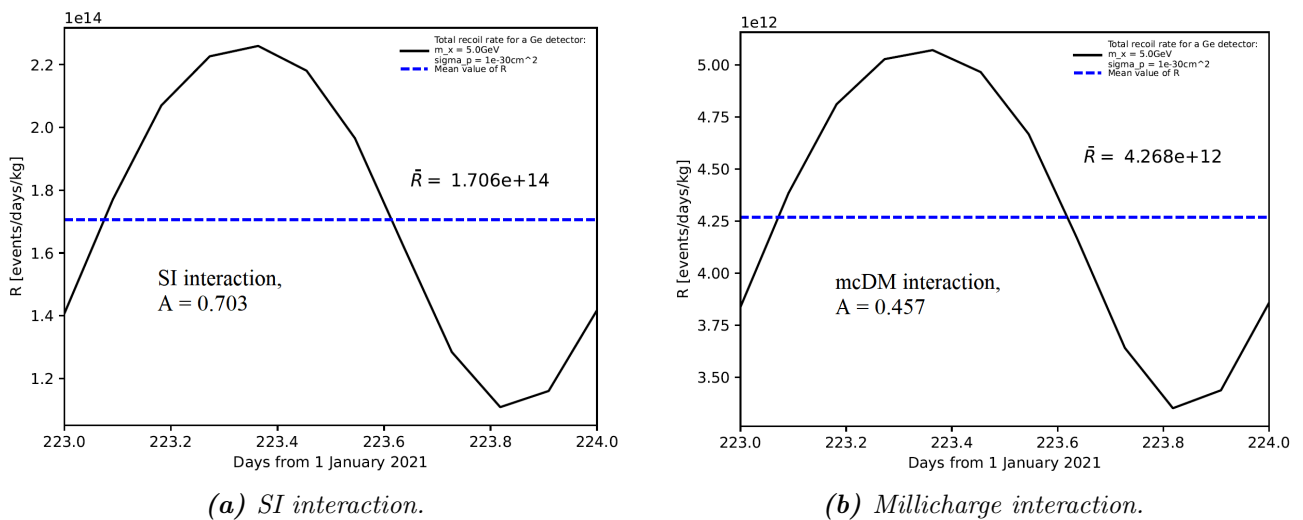


Figure 4.2. Example plot of two DM signals. Detected at the same location (**North**) and depth (**1m**).

We can see that both signals look fairly similar, at least in the functional form. We can see that the average rate is in fact lower for the mcDM case, as expected by looking at the differential recoil rates.

In the following plots, however, we will see that the differential recoil rate, and thus the total rate, falls a lot with respect to the SI interacting DM case. This may be due to the fact that what we are doing is use the same mass and cross section for both plots. As we've increased the DM mass, but not the corresponding cross section, the particles considered here for the SI case are less efficient in transferring energy when compared to the examples that we have given with $m_\chi = 0.1\text{GeV}$. This means that, even if the mcDM particles are greatly attenuated, the ordinary DM particles will not.

If that effect has not become apparent in figure 4.2 may be because of the choice of γ that we are using. Note (from figure 4.1b, for example) that the first considered γ is of about 90° , which means that γ is only running over the northern hemisphere (remember that $\gamma = 180^\circ$ when the average flux of particles are coming from above). Thus, it is expected that for a detector at the northern hemisphere and almost at surface level the attenuation of the signal is small.

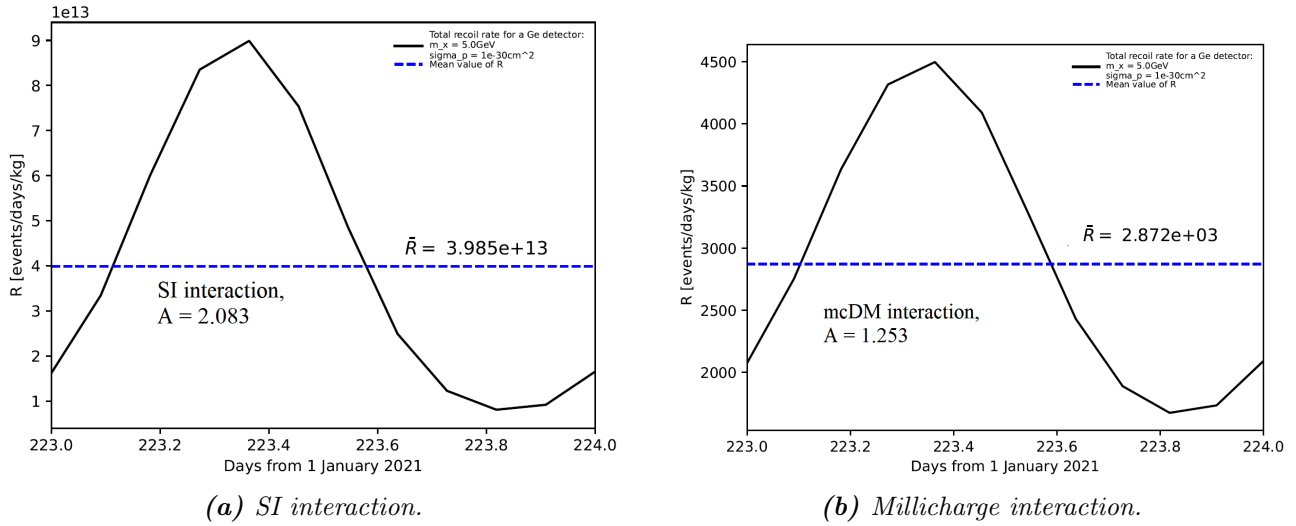


Figure 4.3. Example plot of two DM signals. Detected at the same location (**South**) and depth (**1m**).

We now could say that the signals which differ the most in amplitude would yield the perfect spot for placing a detector but the truth is that, as we have not been able to select a set of ideal parameters, the information that we extract from these plots has to be taken with care.

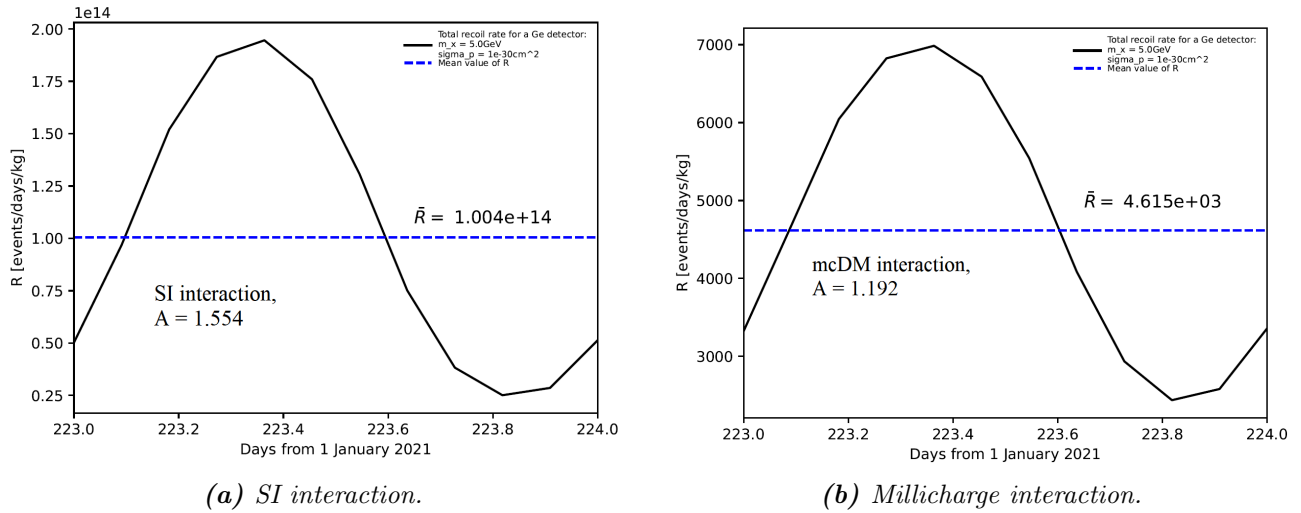


Figure 4.4. Example plot of two DM signals. Detected at the same location (**Equator**) and depth (**1m**).

A way in which we could fix this would be to do a more careful study beforehand on which parameters may yield a better situation like, for example, having both curves with the same average rate. However, by looking at the different amplitudes that we have obtained, it seems safe to say that a more careful and more dedicated analysis could use this technique to distinguish between the ordinary and *millicharge* DM signals.

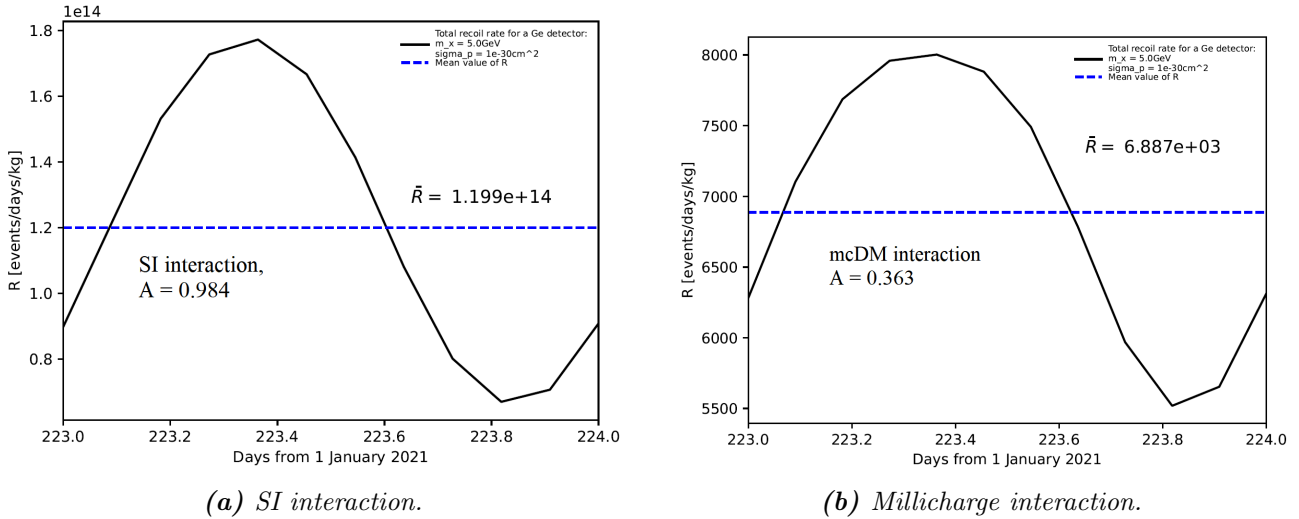


Figure 4.5. Example plot of two DM signals. Detected at the same location (*North*) and depth (*10m*).

4.3 Constraints

The values that we have chosen for the mass and the reference cross section yielded (from Eq. 3.5) a value of the *millicharge* of $\epsilon \approx 3.5 \cdot 10^{-11}$. We can take a look at some constraint plots so that we can check whether the values of the chosen parameters are within the reasonable.

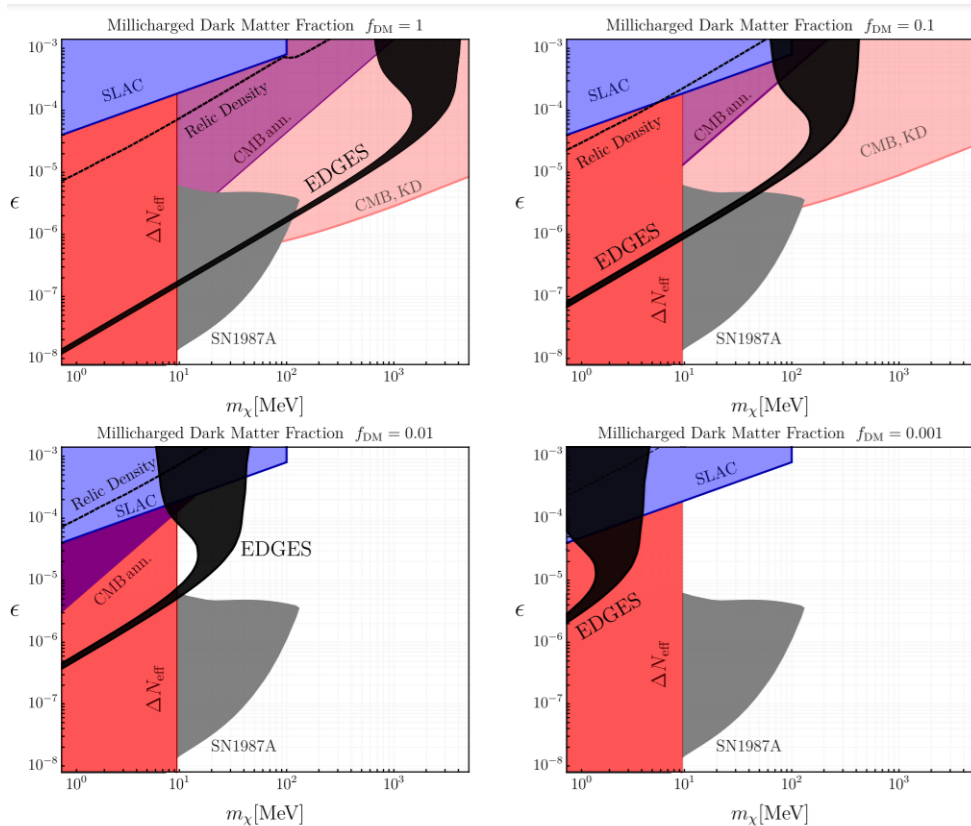


Figure 4.6. Constraints on the value of the millicharge via different experiments, each with a different color. The four plots respond to different fractions of millicharge DM with respect to the total quantity of DM in the univers ($f=1$ is that millicharge DM represents 100% and so on).

As we can see in the figure above, the parameter space is free from exclusion in all of the four plots, which means that the method proposed in this work may be useful to probe down the parameter space in that particular region.

Chapter 5

Discussion and conclusions

In this project, we have proposed a novel way in which we could distinguish signals coming from two very different DM candidates, with very different differential cross sections. For that, we have learned some scattering theory, which is not given in the Bachelor's degree, and we have derived relevant equations which have served us to analyze the whole scattering process, remarkably the two equations for dv/dD .

Also, we've gone through relevant concepts, such as the efficiency of energy transfer between colliding particles or the suppression of the probability of interaction due to the coherence effect, which can be easily translated to other fields of physics.

As we have already stated, the last analysis could have been more thorough in order for us to obtain more meaningful information; however, it is clear that with this method the two signals considered can be distinguished, which is already an achievement.

Another way in which this kind of experiment could be carried out is by considering a directional detector, thus considering the three dimensional velocity distribution of the incoming DM particles, instead of the one-parameter distribution that we have used. This would most certainly give us much more information than the current study at the cost of becoming a much more advanced work.

In general lines, the project has been useful for the student to introduce himself in a new fascinating field of physics, and also for him to learn programming in python, a versatile and directed to science programming language, so the pedagogical value of the project has been met.

Bibliography

- [1] N. Aghanim et al. “Planck 2018 results”. In: *Astronomy Astrophysics* 641 (Sept. 2020), A6. ISSN: 1432-0746. DOI: [10.1051/0004-6361/201833910](https://doi.org/10.1051/0004-6361/201833910). URL: <http://dx.doi.org/10.1051/0004-6361/201833910>.
- [2] F. Zwicky. “Die Rotverschiebung von extragalaktischen Nebeln”. In: *Helvetica Physica Acta* 6 (Jan. 1933), pp. 124–126.
- [3] J. G. de Swart, G. Bertone, and J. van Dongen. “How dark matter came to matter”. In: *Nature Astronomy* 1.3 (Mar. 2017). ISSN: 2397-3366. DOI: [10.1038/s41550-017-0059](https://doi.org/10.1038/s41550-017-0059). URL: <http://dx.doi.org/10.1038/s41550-017-0059>.
- [4] Vera C. Rubin and Jr. Ford W. Kent. “Rotation of the Andromeda Nebula from a Spectroscopic Survey of Emission Regions”. In: 159 (Feb. 1970), p. 379. DOI: [10.1086/150317](https://doi.org/10.1086/150317).
- [5] P.A. Zyla et al. “Review of Particle Physics”. In: *PTEP* 2020.8 (2020), p. 083C01. DOI: [10.1093/ptep/ptaa104](https://doi.org/10.1093/ptep/ptaa104).
- [6] Richard Massey, Thomas Kitching, and Johan Richard. “The dark matter of gravitational lensing”. In: *Reports on Progress in Physics* 73.8 (July 2010), p. 086901. ISSN: 1361-6633. DOI: [10.1088/0034-4885/73/8/086901](https://doi.org/10.1088/0034-4885/73/8/086901). URL: <http://dx.doi.org/10.1088/0034-4885/73/8/086901>.
- [7] M. Ackermann et al. “Searching for Dark Matter Annihilation from Milky Way Dwarf Spheroidal Galaxies with Six Years of Fermi Large Area Telescope Data”. In: *Physical Review Letters* 115.23 (Nov. 2015). ISSN: 1079-7114. DOI: [10.1103/PhysRevLett.115.231301](https://doi.org/10.1103/PhysRevLett.115.231301). URL: <http://dx.doi.org/10.1103/PhysRevLett.115.231301>.
- [8] Matthias Danninger and Kahae Han. *Search for the Kaluza-Klein Dark Matter with the AMANDA/IceCube Detectors*. 2009. arXiv: [0906.3969](https://arxiv.org/abs/0906.3969) [[astro-ph.HE](https://arxiv.org/abs/0906.3969)].
- [9] M. Aguilar et al. “First Result from the Alpha Magnetic Spectrometer on the International Space Station: Precision Measurement of the Positron Fraction in Primary Cosmic Rays of 0.5–350 GeV”. In: *Phys. Rev. Lett.* 110 (14 Apr. 2013), p. 141102. DOI: [10.1103/PhysRevLett.110.141102](https://doi.org/10.1103/PhysRevLett.110.141102). URL: <https://link.aps.org/doi/10.1103/PhysRevLett.110.141102>.
- [10] Gianfranco Bertone et al. “Identifying WIMP dark matter from particle and astroparticle data”. In: *Journal of Cosmology and Astroparticle Physics* 2018.03 (Mar. 2018), pp. 026–026. ISSN: 1475-7516. DOI: [10.1088/1475-7516/2018/03/026](https://doi.org/10.1088/1475-7516/2018/03/026). URL: <http://dx.doi.org/10.1088/1475-7516/2018/03/026>.
- [11] M. Markevitch et al. “Direct Constraints on the Dark Matter Self-Interaction Cross Section from the Merging Galaxy Cluster 1E 0657-56”. In: *The Astrophysical Journal* 606.2 (May 2004), pp. 819–824. DOI: [10.1086/383178](https://doi.org/10.1086/383178). URL: <https://doi.org/10.1086/383178>.
- [12] Marco Taoso, Gianfranco Bertone, and Antonio Masiero. “Dark matter candidates: a ten-point test”. In: *Journal of Cosmology and Astroparticle Physics* 2008.03 (Mar. 2008), p. 022. ISSN: 1475-7516. DOI: [10.1088/1475-7516/2008/03/022](https://doi.org/10.1088/1475-7516/2008/03/022). URL: <http://dx.doi.org/10.1088/1475-7516/2008/03/022>.

- [13] Miguel A. Monroy-Rodríguez and Christine Allen. “THE END OF THE MACHO ERA, REVISITED: NEW LIMITS ON MACHO MASSES FROM HALO WIDE BINARIES”. In: *The Astrophysical Journal* 790.2 (July 2014), p. 159. ISSN: 1538-4357. DOI: [10.1088/0004-637x/790/2/159](https://doi.org/10.1088/0004-637x/790/2/159). URL: <http://dx.doi.org/10.1088/0004-637X/790/2/159>.
- [14] Samuel D. McDermott, Hai-Bo Yu, and Kathryn M. Zurek. “Turning off the lights: How dark is dark matter?” In: *Physical Review D* 83.6 (Mar. 2011). ISSN: 1550-2368. DOI: [10.1103/physrevd.83.063509](https://doi.org/10.1103/physrevd.83.063509). URL: <http://dx.doi.org/10.1103/PhysRevD.83.063509>.
- [15] Gianfranco Bertone, Dan Hooper, and Joseph Silk. “Particle dark matter: evidence, candidates and constraints”. In: *Physics Reports* 405.5-6 (Jan. 2005), pp. 279–390. ISSN: 0370-1573. DOI: [10.1016/j.physrep.2004.08.031](https://doi.org/10.1016/j.physrep.2004.08.031). URL: <http://dx.doi.org/10.1016/j.physrep.2004.08.031>.
- [16] Anne M Green and Bradley J Kavanagh. “Primordial black holes as a dark matter candidate”. In: *Journal of Physics G: Nuclear and Particle Physics* 48.4 (Feb. 2021), p. 043001. ISSN: 1361-6471. DOI: [10.1088/1361-6471/abc534](https://doi.org/10.1088/1361-6471/abc534). URL: <http://dx.doi.org/10.1088/1361-6471/abc534>.
- [17] Sean Fraser et al. “The EDGES 21 cm anomaly and properties of dark matter”. In: *Physics Letters B* 785 (Oct. 2018), pp. 159–164. ISSN: 0370-2693. DOI: [10.1016/j.physletb.2018.08.035](https://doi.org/10.1016/j.physletb.2018.08.035). URL: <http://dx.doi.org/10.1016/j.physletb.2018.08.035>.
- [18] Asher Berlin et al. “Severely Constraining Dark-Matter Interpretations of the 21-cm Anomaly”. In: *Physical Review Letters* 121.1 (July 2018). ISSN: 1079-7114. DOI: [10.1103/physrevlett.121.011102](https://doi.org/10.1103/physrevlett.121.011102). URL: <http://dx.doi.org/10.1103/PhysRevLett.121.011102>.
- [19] Bradley J. Kavanagh. “Earth scattering of superheavy dark matter: Updated constraints from detectors old and new”. In: *Physical Review D* 97.12 (June 2018). ISSN: 2470-0029. DOI: [10.1103/physrevd.97.123013](https://doi.org/10.1103/physrevd.97.123013). URL: <http://dx.doi.org/10.1103/PhysRevD.97.123013>.
- [20] B.J. Kavanagh. “Verne”. In: *Astrophysics Source Code Library* (2017). DOI: [doi:10.5281/zenodo.1115601](https://doi.org/10.5281/zenodo.1115601). URL: <https://github.com/bradkav/verne>.
- [21] Mark Thomson. *Modern Particle Physics*. Cambridge University Press, 2013. DOI: [10.1017/CBO9781139525367](https://doi.org/10.1017/CBO9781139525367).
- [22] David G. Cerdeño and Anne M. Green. “Direct detection of WIMPs”. In: (Feb. 2010). arXiv: [1002.1912](https://arxiv.org/abs/1002.1912) [[astro-ph.CO](https://arxiv.org/abs/1002.1912)].
- [23] J.D. Lewin and P.F. Smith. “Review of mathematics, numerical factors, and corrections for dark matter experiments based on elastic nuclear recoil”. In: *Astroparticle Physics* 6.1 (1996), pp. 87–112. ISSN: 0927-6505. DOI: [https://doi.org/10.1016/S0927-6505\(96\)00047-3](https://doi.org/10.1016/S0927-6505(96)00047-3). URL: <https://www.sciencedirect.com/science/article/pii/S0927650596000473>.
- [24] Gintaras Dūda, Ann Kemper, and Paolo Gondolo. “Model-independent form factors for spin-independent neutralino–nucleon scattering from elastic electron scattering data”. In: *Journal of Cosmology and Astroparticle Physics* 2007.04 (Apr. 2007), pp. 012–012. ISSN: 1475-7516. DOI: [10.1088/1475-7516/2007/04/012](https://doi.org/10.1088/1475-7516/2007/04/012). URL: <http://dx.doi.org/10.1088/1475-7516/2007/04/012>.
- [25] Richard H. Helm. “Inelastic and Elastic Scattering of 187-Mev Electrons from Selected Even-Even Nuclei”. In: *Phys. Rev.* 104 (5 Dec. 1956), pp. 1466–1475. DOI: [10.1103/PhysRev.104.1466](https://doi.org/10.1103/PhysRev.104.1466). URL: <https://link.aps.org/doi/10.1103/PhysRev.104.1466>.
- [26] ANNE M. GREEN. “ASTROPHYSICAL UNCERTAINTIES ON DIRECT DETECTION EXPERIMENTS”. In: *Modern Physics Letters A* 27.03 (Jan. 2012), p. 1230004. ISSN: 1793-6632. DOI: [10.1142/s0217732312300042](https://doi.org/10.1142/s0217732312300042). URL: <http://dx.doi.org/10.1142/S0217732312300042>.

- [27] T. Piffi et al. “The RAVE survey: the Galactic escape speed and the mass of the Milky Way”. In: *Astronomy Astrophysics* 562 (Feb. 2014), A91. ISSN: 1432-0746. DOI: [10.1051/0004-6361/201322531](https://doi.org/10.1051/0004-6361/201322531). URL: <http://dx.doi.org/10.1051/0004-6361/201322531>.
- [28] Chris Savage, Katherine Freese, and Paolo Gondolo. “Annual modulation of dark matter in the presence of streams”. In: *Physical Review D* 74.4 (Aug. 2006). ISSN: 1550-2368. DOI: [10.1103/physrevd.74.043531](https://doi.org/10.1103/physrevd.74.043531). URL: <http://dx.doi.org/10.1103/PhysRevD.74.043531>.
- [29] Chris Kelso et al. “The impact of baryons on the direct detection of dark matter”. In: *Journal of Cosmology and Astroparticle Physics* 2016.08 (Aug. 2016), pp. 071–071. ISSN: 1475-7516. DOI: [10.1088/1475-7516/2016/08/071](https://doi.org/10.1088/1475-7516/2016/08/071). URL: <http://dx.doi.org/10.1088/1475-7516/2016/08/071>.
- [30] E. Aprile et al. “Search for Light Dark Matter Interactions Enhanced by the Migdal Effect or Bremsstrahlung in XENON1T”. In: *Physical Review Letters* 123.24 (Dec. 2019). ISSN: 1079-7114. DOI: [10.1103/physrevlett.123.241803](https://doi.org/10.1103/physrevlett.123.241803). URL: <http://dx.doi.org/10.1103/PhysRevLett.123.241803>.
- [31] F. Mayet et al. “A review of the discovery reach of directional Dark Matter detection”. In: *Physics Reports* 627 (Apr. 2016), pp. 1–49. ISSN: 0370-1573. DOI: [10.1016/j.physrep.2016.02.007](https://doi.org/10.1016/j.physrep.2016.02.007). URL: <http://dx.doi.org/10.1016/j.physrep.2016.02.007>.
- [32] D. Abrams et al. “Exclusion limits on the WIMP-nucleon cross section from the Cryogenic Dark Matter Search”. In: *Physical Review D* 66.12 (Dec. 2002). ISSN: 1089-4918. DOI: [10.1103/physrevd.66.122003](https://doi.org/10.1103/physrevd.66.122003). URL: <http://dx.doi.org/10.1103/PhysRevD.66.122003>.
- [33] G. Angloher et al. “Results on MeV-scale dark matter from a gram-scale cryogenic calorimeter operated above ground”. In: *The European Physical Journal C* 77.9 (Sept. 2017). ISSN: 1434-6052. DOI: [10.1140/epjc/s10052-017-5223-9](https://doi.org/10.1140/epjc/s10052-017-5223-9). URL: <http://dx.doi.org/10.1140/epjc/s10052-017-5223-9>.
- [34] Timon Emken and Chris Kouvaris. “How blind are underground and surface detectors to strongly interacting dark matter?” In: *Physical Review D* 97.11 (June 2018). ISSN: 2470-0029. DOI: [10.1103/physrevd.97.115047](https://doi.org/10.1103/physrevd.97.115047). URL: <http://dx.doi.org/10.1103/PhysRevD.97.115047>.
- [35] Standard International Organization for Standardization. *Standard Atmosphere*. 1975. URL: <https://www.iso.org/standard/7472.html> (visited on 09/17/2021).
- [36] Johan Lundberg and Joakim Edsjö. “Weakly interacting massive particle diffusion in the solar system including solar depletion and its effect on Earth capture rates”. In: *Physical Review D* 69.12 (June 2004). ISSN: 1550-2368. DOI: [10.1103/physrevd.69.123505](https://doi.org/10.1103/physrevd.69.123505). URL: <http://dx.doi.org/10.1103/PhysRevD.69.123505>.
- [37] M. Shafi Mahdawi and Glennys R. Farrar. “Constraints on Dark Matter with a moderately large and velocity-dependent DM-nucleon cross-section”. In: *Journal of Cosmology and Astroparticle Physics* 2018.10 (Oct. 2018), pp. 007–007. ISSN: 1475-7516. DOI: [10.1088/1475-7516/2018/10/007](https://doi.org/10.1088/1475-7516/2018/10/007). URL: <http://dx.doi.org/10.1088/1475-7516/2018/10/007>.